

# An expanded catalogue of low surface brightness galaxies in the Coma cluster using Subaru/Suprime-Cam

Adebusola B. Alabi<sup>1,3\*</sup>, Aaron J. Romanowsky<sup>1,2</sup>, Duncan A. Forbes<sup>3</sup>, Jean P. Brodie<sup>1,3</sup>, Nobuhiro Okabe<sup>4,5,6</sup>

<sup>1</sup> University of California Observatories, 1156 High Street, Santa Cruz, CA 95064, USA

<sup>2</sup> Department of Physics and Astronomy, San José State University, San Jose, CA 95192, USA

<sup>3</sup> Centre for Astrophysics & Supercomputing, Swinburne University, Hawthorn VIC 3122, Australia

<sup>4</sup> Department of Physical Science, Hiroshima University, 1-3-1, Kagamiyama, Higashi-Hiroshima, Hiroshima 739-8526, Japan

<sup>5</sup> Hiroshima Astrophysical Science Center, Hiroshima University, 1-3-1, Kagamiyama, Higashi-Hiroshima, Hiroshima 739-8526, Japan

<sup>6</sup> Core Research for Energetic Universe, Hiroshima University, 1-3-1, Kagamiyama, Higashi-Hiroshima, Hiroshima 739-8526, Japan

Accepted today

## ABSTRACT

We present a catalogue of low surface brightness (LSB) galaxies in the Coma cluster obtained from deep Subaru/Suprime-Cam *V* and *R*-band imaging data within a region of  $\sim 4$  deg<sup>2</sup>. We increase the number of LSB galaxies presented in Yagi et al. (2016) by a factor of  $\sim 3$  and report the discovery of 29 new ultra-diffuse galaxies (UDGs). We compile the largest sample of ultra-diffuse galaxies with colours and structural parameters in the Coma cluster. While most UDGs lie along the red-sequence relation of the colour–magnitude diagram,  $\sim 16$  per cent are outside (bluer or redder) the red-sequence region of Coma cluster galaxies. Our analyses show that there is no special distinction in the basic photometric parameters between UDGs and other LSB galaxies. We investigate the clustercentric colour distribution and find a remarkable transition at a projected radius of  $\sim 0.6$  Mpc. Within this cluster core region and relative to the red-sequence of galaxies, LSB galaxies are on average redder than co-spatial higher surface brightness galaxies at the  $2\sigma$  level, highlighting how vulnerable LSB galaxies are to the physical processes at play in the dense central region of the cluster. The position of the transition radius agrees with expectations from recent cosmological simulation of massive galaxy clusters within which ancient infalls are predicted to dominate the LSB galaxy population.

**Key words:** galaxies: catalogues – galaxies: clusters: individual (Coma) – galaxies: photometry – galaxies: fundamental parameters

## 1 INTRODUCTION

There has been a rekindling of interest in low surface brightness (LSB) galaxies with the recent discovery of ultra-diffuse galaxies (UDGs) in the Coma cluster. UDGs are extended LSB galaxies with effective radii  $R_e \gtrsim 1.5$  kpc, central surface brightnesses  $\mu(g, 0) \gtrsim 24$  mag arcsec<sup>-2</sup>, and exponential light profiles, i.e. Sérsic index,  $n \sim 1$ . The first 47 UDGs were catalogued by van Dokkum et al. (2015), mostly outside the cluster core, using the remarkable Dragonfly Telephoto Array (Abraham & van Dokkum 2014). Several groups have since reported the discovery of more UDGs in the Coma cluster (e.g., Koda et al. 2015; Yagi et al. 2016; Ruiz-Lara et al. 2018a; Zaritsky et al. 2019; Chilingarian et al. 2019). To date,  $\sim 30$  Coma cluster UDGs have been spectroscopically confirmed as

cluster members (Kadowaki et al. 2017; Alabi et al. 2018; Ruiz-Lara et al. 2018a; Chilingarian et al. 2019).

While the debate about the true origin and nature of these enigmatic galaxies still persists in the literature, we note that most of the Coma cluster UDGs still lack colour information: a fundamental diagnostic in understanding the formation and evolution of galaxies (Renzini 2006). This omission may be directly linked to the fact that most of the UDG discoveries were made from analysis of single-band photometry and that faint photometry is challenging. Only 52 UDGs out of the 854 Coma cluster LSB galaxies in the catalogue of Yagi et al. (2016) have  $B - R$  colour measurements, and all within a  $\sim 0.7$  deg<sup>2</sup> area<sup>1</sup>. The faint LSB galaxy catalogue

<sup>1</sup> This is only  $\sim 10$  per cent of the area defined by the projected virial radius of the Coma cluster, i.e.  $\sim 2.9$  Mpc (Kubo et al. 2007)

\* Email: aalabi@ucsc.edu

of [Adami et al. \(2006\)](#) with  $B - R$  colour covers a similarly small central  $\sim 0.6 \text{ deg}^2$  area within the Coma cluster. The recently published SMUDGes catalogue ([Zaritsky et al. 2019](#)), which extends beyond the virial radius of the Coma cluster, has colour measurements available for only 43 UDGs from the [Yagi et al. \(2016\)](#) catalogue. The small sample size and limited radial coverage of Coma cluster UDGs with known colours therefore makes a systematic photometric study that is targeted at UDGs an urgent necessity.

While the environmental variation of galaxy colours with projected distance from the centre of the Coma cluster is well established in the literature for bright galaxies ([Terlevich et al. 2001](#); [Mahajan et al. 2011](#)) and dwarf galaxies ([Secker et al. 1997](#)), the situation for UDGs, and in general, LSB galaxies within the Coma cluster, remains unclear. For example, [Adami et al. \(2006\)](#) did not find any significant variation in colour with clustercentric radius in their faint LSB galaxy sample, perhaps due to the radially limited nature of their data. [Terlevich et al. \(2001\)](#) attributed the blueing of mean galaxy colours with projected distance from the centre of the Coma cluster to an age effect, i.e., the cluster core is dominated by redder galaxies with older stellar ages, while the outskirts region is dominated by bluer galaxies with younger stellar ages. This is consistent with results from the spectroscopic studies of [Smith et al. \(2009\)](#) and [Smith et al. \(2011\)](#), although [Carter et al. \(2002\)](#) claimed that the environmental colour trends could also be a metallicity effect. [Smith et al. \(2011\)](#) additionally showed that low mass galaxies have steeper radial age trends compared to their more massive counterparts. There are indications that UDGs (and by extension LSB galaxies) may have a similar clustercentric trends to dwarf galaxies ([Román & Trujillo 2017](#); [Alabi et al. 2018](#); [Ferre-Mateu et al. 2018](#); [Mancera Pia et al. 2019](#); [Zaritsky et al. 2019](#); [Chilingarian et al. 2019](#)) but the true behaviour within the Coma cluster is still unknown due to the paucity of UDGs with optical colour data.

Furthermore, while the vast majority of cluster UDGs are quiescent and lie on the red-sequence of the colour–magnitude relation ([Koda et al. 2015](#)), a few UDGs with significant deviations from the red-sequence –mostly bluewards– have been reported ([Román & Trujillo 2017](#); [Chilingarian et al. 2019](#); [Zaritsky et al. 2019](#)), mostly in low density environments including the cluster outskirts ([Alabi et al. 2018](#)). [Adami et al. \(2006\)](#) previously identified faint LSB galaxies in the Coma cluster with colours redder or bluer than the red-sequence galaxies. They interpreted these faint LSB galaxies as recent cluster infalls from less–dense environments where they have been “pre-processed” to varying degrees ([Zabludoff & Mulchaey 1998](#)). Identifying galaxies that are bluer or redder relative to the red-sequence region from coherent photometry is therefore useful in understanding the origin of present-day cluster LSB galaxies.

In this work, we present a catalogue of galaxies within  $\sim 4 \text{ deg}^2$  of the Coma cluster. We probe the same region of the Coma cluster as in the  $R$ -band LSB galaxy studies of [Koda et al. \(2015\)](#) and [Yagi et al. \(2016\)](#), hitherto the most comprehensive works on Coma cluster LSB galaxies, employing an additional  $V$ -band filter in order to obtain colours and securely discriminate against contamination from background galaxies. We present a description of our imaging data in Section 2. We give details of our data analysis in Sections 3 and 4 including galaxy detection, galaxy modelling with GALFIT, and removal of confirmed contaminants from our catalogue. We present our Coma cluster colour–magnitude diagram in Section 5 and discuss the residual contamination in our final catalogue. Finally, we present our final catalogue and summarize our results in Section 6.

Throughout this work, we adopt a distance of 100 Mpc, a redshift of 0.023, a distance modulus of  $(m - M)_0 = 35$  ([Carter et al. 2008](#)), a virial radius of  $\sim 2.9$  Mpc ([Kubo et al. 2007](#)), position angle of  $71.5 \text{ deg}$  ([Plionis 1994](#)), and central co-ordinates RA:  $12:59:48.75$  and Dec:  $+27:58:50.9$  (J2000) for the Coma cluster. We also adopt the following cosmology:  $\Omega_m = 0.3$ ,  $\Omega_\Lambda = 0.7$  and,  $H_0 = 70 \text{ km s}^{-1} \text{ Mpc}^{-1}$ .

## 2 DATA

We analyse the Coma cluster Subaru/Suprime-Cam ([Miyazaki et al. 2002](#))  $V$  and  $R$  band imaging data previously reduced and published in the weak-lensing study of [Okabe et al. \(2014\)](#). The imaging is made up of a mosaic of 18 individual pointings with  $2'$  overlap between adjacent fields and a total sky coverage of  $\sim 4 \text{ deg}^2$ . Details of the exposure times and seeing per pointing can be found in [Okabe et al. \(2014\)](#) alongside a summary of the data reduction process. Average exposure time and seeing FWHM are 14 minutes &  $1''$  and 26 minutes &  $0.7''$ , in the  $V$  and  $R$ -bands, respectively. We note that our  $R$ -band imaging is slightly different from that used by [Yagi et al. \(2016, hereafter Y16\)](#), where they included additional imaging data with worse seeing in 4 pointings in their analysis. Figure 1 shows the mosaic of the 18 pointings and the overlapping regions between them.

We used the publicly available code by [Kelly et al. \(2014\)](#) to check and confirm the zero-point magnitudes originally used for photometric calibration by [Okabe et al. \(2014\)](#) using bright stars in common with the Sloan Digital Sky Survey (SDSS) catalogue ([Ahn et al. 2012](#)). Our zero-points are similar to those obtained by [Okabe et al. \(2014\)](#). We apply Galactic extinction corrections on a per-pointing basis to the magnitude and surface brightness measurements, using values from the dust extinction maps of [Schlafly & Finkbeiner \(2011\)](#). This is because extinction variation from object to object within the same pointing is very small compared to the estimated photometric uncertainties (see Section 4.3 for more details). The applied corrections vary from 0.021–0.033 mag and 0.017–0.026 mag in the  $V$  and  $R$  bands, respectively. We also applied “K-corrections” of 0.03 and 0.02 to  $V$  and  $R$ -band photometry, respectively, determined using the K-corrections calculator ([Chilingarian et al. 2010](#); [Chilingarian & Zolotukhin 2012](#)). All magnitudes hereafter are in the AB system, and are extinction and K-corrected.

## 3 OBJECT DETECTION

We perform initial object detection on both  $V$  and  $R$ -band images with SExtractor ([Bertin & Arnouts 1996](#)), adjusting the configuration criteria to maximize the detection of galaxies from the Coma cluster low surface brightness catalogue of Y16. We run SExtractor in the “dual-image” mode, using the  $R$ -band imaging for object detection and use the following criteria, similar to that used in Y16, to identify galaxy candidates in our SExtractor catalogue:

- non-zero SExtractor Petrosian RADIUS,
- SExtractor FWHM  $\geq 5$  pixels ( $\sim 0.5 \text{ kpc}$  at the distance of Coma cluster),
- SExtractor FLAG parameter  $< 4$  (objects with defects such as saturated pixels or truncated isophotes are excluded),
- SExtractor CLASS\_STAR parameter  $< 0.5$  (objects with CLASS\_STAR  $\sim 1$  are foreground stars),

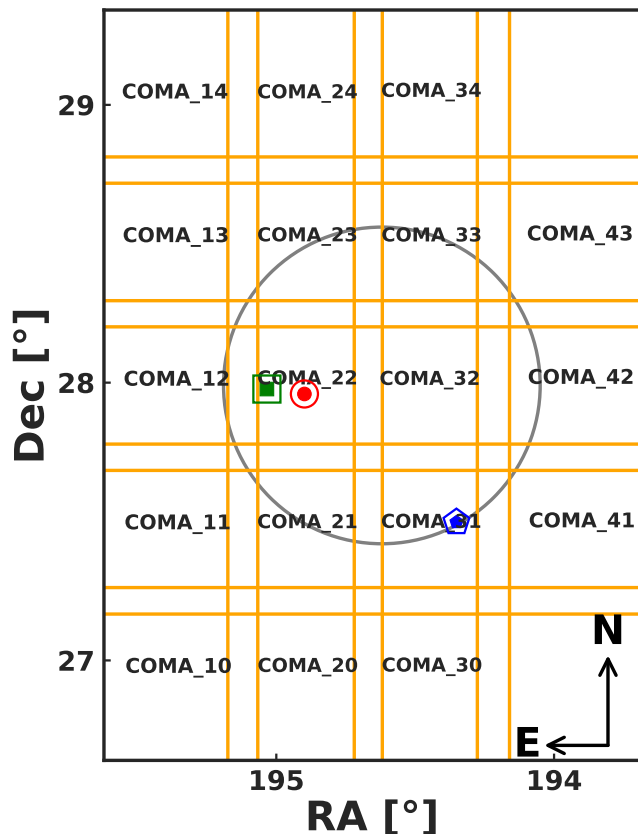


**Figure 1.** Mosaic of the 18 pointings used to observe the Coma cluster. The final mosaic covers  $\sim 4.2^\circ$  region of the Coma cluster. Galaxy IDs in the final catalogue are prefixed with the names of their originating pointing as shown in the plot. Multiple galaxy detections from the overlapping regions between adjacent pointings are used later in the text to quantify reliable uncertainties on the modelled galaxy structural parameters. As a guide to the physical scale, we show a circle with projected radius of 1 Mpc within which we have marked the positions of the three cD galaxies: NGC 4889 (green square), NGC 4874 (red circle), and NGC 4839 (blue pentagon).

- $R$ -band magnitude uncertainty  $< 0.2$  (this corresponds to a minimum signal-to-noise ratio (SNR)  $\sim 5$ ).

This initial list of criteria help to exclude spurious detections, foreground stars, unresolved compact sources (globular clusters), and some background galaxies from our catalogue, reducing the size of our SExtractor source list by a factor of  $\sim 4$  to  $\sim 200,000$  objects.

Next, we use the peak surface brightness – magnitude diagram as a diagnostic to further remove contaminants from our sample of galaxy candidates. As shown in Figure 2, galaxies that belong to the Coma cluster tend to occupy a distinct region compared to the fainter background galaxies. We compile and show a sample of confirmed Coma cluster galaxies from the literature which we match to our object catalogue. These galaxies vary from giants to dwarf galaxies and are selected from the spectroscopic studies of Mobasher et al. (2001), Edwards et al. (2002), Aguerri et al. (2005), Smith et al. (2009), the NASA/IPAC Extragalactic Database (NED)<sup>2</sup> Coma cluster galaxy list, and SDSS. The com-

<sup>2</sup> <http://ned.ipac.caltech.edu/>

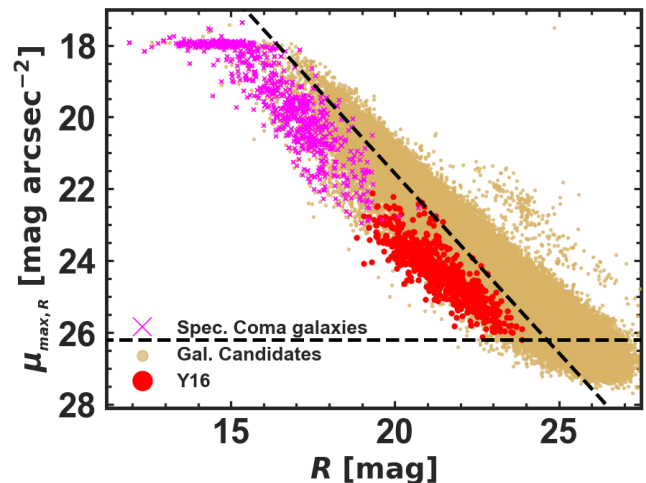


**Figure 2.** Peak surface brightness– $R$ -band magnitude diagram showing Coma cluster galaxy candidates (brown dots) from our SExtractor analysis. We also show spectroscopically confirmed Coma cluster galaxies from various sources in the literature (magenta X's). At any surface brightness, likely Coma cluster galaxies have brighter apparent magnitudes. The inclined line shows the expected peak surface brightness for a galaxy with  $R_e \sim 1.2''$  (the worst FWHM seeing in our imaging data equivalent to  $\sim 0.6$  kpc at the distance of Coma cluster), while the horizontal line is our faint peak surface brightness limit ( $\sim 26.1$  mag arcsec $^{-2}$ ), defined using the low surface brightness catalogue of Yagi et al. (2016, Y16) (red dots). Galaxy candidates with saturated central pixels around  $\mu_{max,R} \sim 18.1$  mag arcsec $^{-2}$  are excluded from subsequent analysis. The magnitudes shown here and hereafter have all been corrected for Galactic extinction and are  $K$ -corrected.

pilation, however, contains only bright galaxies, i.e.  $R \leq 19$  mag, which have been the traditional subjects of spectroscopic studies. We extend this sample to fainter magnitudes ( $R \sim 24$  mag) by including the LSB galaxies from Y16, which have been shown to be mostly cluster members in various studies (e.g. Kadowaki et al. 2017; Alabi et al. 2018; Ruiz-Lara et al. 2018b; Chilingarian et al. 2019).

The inclined line shows the expected peak surface brightness for a galaxy with  $R_e \sim 1.2''$  assuming an exponential profile, i.e. Sérsic index,  $n = 1$ , (the worst FWHM seeing in the  $V$ -band equivalent to 0.6 kpc at the distance of the Coma Cluster) at various magnitudes. We therefore exclude galaxy detections smaller than this size-limit from subsequent analysis, since they are most likely background sources, ultracompact dwarfs, or imaging defects such as false detections in the halos of bright stars. Likewise, we use the LSB catalogue of Y16 to define the faint surface brightness limit of our catalogue. We adopt a peak surface brightness limit of  $\mu_{max,R} \sim 26.1$  mag arcsec $^{-2}$  which is equivalent to a mean effective surface brightness of 27.2 mag arcsec $^{-2}$ . We also exclude all galaxy candidates (209) with saturated central pixels seen around  $\mu_{max,R} \sim 18.1$  mag arcsec $^{-2}$ . With the application of these thresholds, the size of our catalogue is now reduced to 27,437 galaxies which is better suited for subsequent GALFIT analysis, including 1,305 galaxies detected in more than one pointing. Likewise, out of the 854 LSB galaxies published in Y16, our catalogue contains 757 galaxies with detection in both bands, alongside 181 duplicate detections. We later use these duplicate detections to estimate the true uncertainties on the structural parameters of our galaxies.

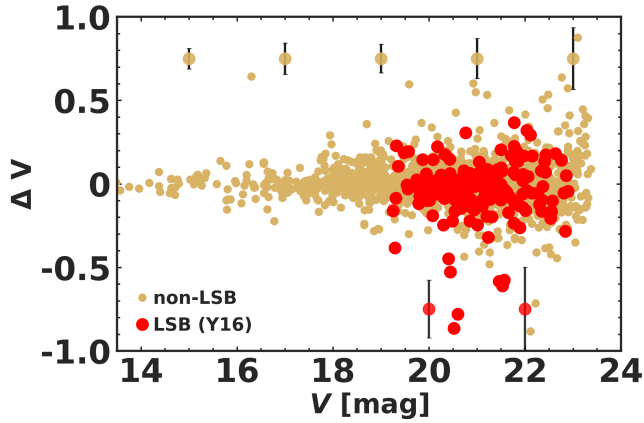


**Figure 3.** Variation in GALFIT  $V$ -band magnitude measurements in the 1,305 galaxies with duplicate detections. We show the low surface brightness galaxies from the catalogue of Y16 as red circles, while the remaining cluster galaxies are shown as smaller brown circles. The corresponding error-bars are the standard deviations determined in magnitude bins of width  $\Delta V = 2$  mag and they increase up to a maximum of  $\sim 0.5$  at very faint magnitudes.

#### 4 GALAXY MODELLING WITH GALFIT

The projected intensity profile,  $I(R)$ , of a galaxy can be described with a Sérsic function (Sérsic 1968; Graham & Driver 2005) of the form:

$$I(R) = I_e \exp \left[ -b_n \left( \left( \frac{R}{R_e} \right)^{1/n} - 1 \right) \right] \quad (1)$$

where  $I_e$  is the intensity at the effective radius  $R_e$  which encloses half the total galaxy luminosity,  $n$  is the Sérsic index, also known as the profile shape parameter, and  $b_n$  is a complicated function of  $n$ . Bright elliptical galaxies which are centrally concentrated typically follow de Vaucouleurs profiles (de Vaucouleurs 1948, 1959) with  $n \sim 4$ , while the less centrally concentrated spiral disks and LSB galaxies have exponential profiles with  $n \sim 1$ .

To obtain the structural properties of all the galaxies in our catalogue, we fit Sérsic functions in both  $V$  and  $R$  bands independently with GALFIT<sup>3</sup> (Peng et al. 2010). We make postage-stamp cutouts for each galaxy candidate using the positions and size estimates from our initial SExtractor analysis as a basis. Each cutout is centred on the central pixel coordinates from SExtractor with dimensions set to 10 times the  $R_e$  to allow for good sky estimation. We then identify and mask out all bright sources within the frame that do not belong to the target galaxy in an automated way. We jointly fit for the position, magnitude,  $R_e$ ,  $n$ , axis ratio ( $q$ ), and position angle ( $PA$ ) of the target galaxy, as well as the sky background value. Point-spread functions (PSF) used in the fitting process are constructed for each pointing from a sample of bright, unsaturated stars (on average, we use  $\sim 50$  stars per pointing), pre-selected from Section 3.

##### 4.1 Quality Control

In order to identify galaxies with reliable structural parameters, we compare the formal uncertainties on the magnitudes obtained from

GALFIT with estimates of their systematic errors. We obtain these systematic errors from the sample of galaxies with duplicate observations and require that for a good fit, the formal uncertainties should be less than the systematic errors (Häussler et al. 2007). This requirement implies that the uncertainties on the magnitude measurements are never dominated by pixel noise.

Figure 3 shows how  $V$ -band magnitude measurements differ in galaxies with duplicate detections. At fainter magnitudes and in the LSB galaxies, where SNR is significantly reduced and galaxy edges are difficult to identify, the differences between duplicate measurements are significantly increased, reaching  $\sim 0.5$  mag. We use the standard deviations of these distributions, i.e.,  $\sigma_{\Delta V} \sim 0.16$ ;  $\sigma_{\Delta R} \sim 0.20$ , as limits in determining good and acceptable fits. This, in addition to a visual examination of the fits, reduces the size of our Coma cluster catalogue to 11,496 galaxies. A visual examination of all the discarded galaxy candidates reveal that most of them are either spurious detections, typically, with extremely large  $n$  values and smaller  $R_e$  or faint sources in heavily crowded fields.

##### 4.2 Correction to total magnitudes

Since the galaxy-background boundary is not as well-defined in LSB galaxies compared to their HSB counterparts (e.g. Trujillo et al. 2001; Adami et al. 2006; Häussler et al. 2007; Wittmann et al. 2017), we investigate how robust the total magnitudes from GALFIT analysis are by also obtaining their curve-of-growth (COG) total magnitudes. We fix the position,  $q$ , and  $PA$  to parameter values from our previous GALFIT analysis and estimate the total magnitudes within consecutive isophotes, starting from  $0.25R_e$ , and moving outwards in steps of 3 pixels, i.e., 0.3 kpc, stopping when the magnitude difference between successive isophotes is  $< 0.02$  mag. We exclude galaxies that have nearby neighbors within a radius of  $7R_e$  from this analysis.

This exercise shows that the total integrated magnitude from GALFIT is systematically fainter than the asymptotic magnitude from the COG analysis, with the corrections becoming significant in both  $V$  and  $R$  bands, i.e.,  $\geq 0.2$  mag, only when the mean galaxy surface brightness is fainter than  $\sim 24$  mag arcsec<sup>-2</sup>. We show the mean magnitude corrections as a function of mean effective surface brightness in Figure 4 and fit linear functions which we apply to total magnitudes from GALFIT analysis.

$$\begin{aligned} \Delta V &= 0.037 \times \langle \mu_{\text{eff},V} \rangle - 0.67 \\ \Delta R &= 0.044 \times \langle \mu_{\text{eff},R} \rangle - 0.82 \end{aligned} \quad (2)$$

##### 4.3 Estimation of true uncertainties on structural parameters

As already mentioned in Section 4.1, the formal errors from GALFIT are significantly lower than the systematic errors obtained from duplicate detections, at least for the total magnitudes. The formal uncertainties are based entirely on Poisson pixel noise and may be unrealistic estimates in cases such as when the adopted model does not adequately describe the galaxy light profile or when the boundaries of galaxies are difficult to identify due to low SNR, rapidly varying sky background, or crowding from nearby neighbours.

Figure 5 shows how the deviations between repeat measurements of model parameters for the same galaxies vary as a function of mean surface brightness in both  $V$  and  $R$ -bands. We fit linear

<sup>3</sup> <http://users.obs.carnegiescience.edu/peng/work/galfit>



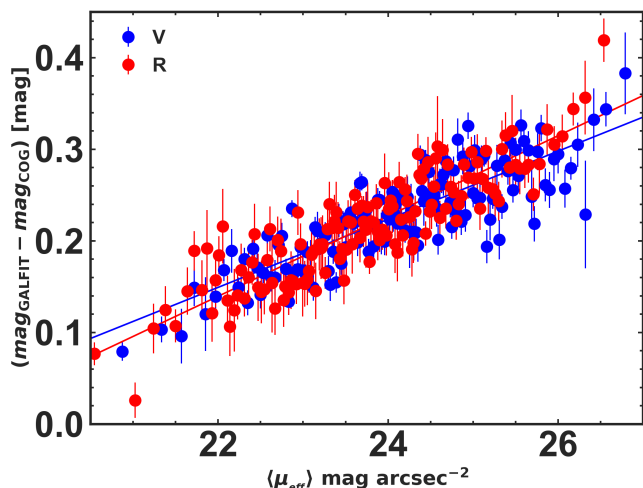


**Figure 4.** Mean offset between total magnitudes from GALFIT and asymptotic magnitudes from curve-of-growth analysis as a function of mean effective surface brightness for galaxies in our sample that are relatively isolated. The magnitude correction factor increases as galaxies become fainter, reaching a maximum of  $\sim 0.4$  mag at  $\sim 27$  mag arcsec $^{-2}$ , where the galaxy-background boundaries become vague.

Parameter	V		R	
	$\alpha$	$\beta$	$\alpha$	$\beta$
mag	0.137	-4.393	0.042	-2.11
$R_e$	0.183	-5.603	0.096	-3.326
Sérsic $n$	0.18	-5.178	0.129	-3.734
$q$	0.248	-4.318	0.085	-3.219
$PA$	0.299	-4.438	0.189	-3.831

**Table 1.** Summary of the coefficients used in eq. 3 to estimate the systematic errors unaccounted for in the GALFIT analysis.

functions of the form

$$\log \sigma = \alpha \times \langle \mu_{\text{eff}} \rangle + \beta \quad (3)$$

to the distribution of the 68th percentile of the difference of each model parameter in bins of mean surface brightness, with  $\alpha$  and  $\beta$  being the fit coefficients, respectively. The best-fitting  $\alpha$  and  $\beta$  coefficients are summarized in Table 1 and are used to compute  $\sigma$  for any measured mean surface brightness. Our final adopted error estimates, shown in Table 2, are obtained by adding  $\sigma$  in quadrature to the GALFIT formal uncertainties.

#### 4.4 Removal of spectroscopic contaminants from the Cluster catalogue

As a final step in minimizing contaminants in our final catalogue, we retrieve spectroscopically confirmed foreground stars and background galaxies (including quasi-stellar objects (QSO)) in the direction of the Coma cluster from the literature. This compilation comes mostly from SDSS and NED (266 foreground stars, 208 QSOs, and 1042 background galaxies) supplemented with 31 and 20 background galaxies from Adami et al. (2009) and Chiboucas et al. (2010), respectively. We also include 2 galaxies from the Y16 LSB catalogue known to be background galaxies (Kad-

owaki et al. 2017; Alabi et al. 2018). This sample, which we compare with our catalogue, is such that the foreground stars have  $-300 \leq V_{\text{los}} [\text{km s}^{-1}] \leq 300$ , the QSOs  $V_{\text{los}} \geq 30000 \text{ km s}^{-1}$ , while the background galaxies have  $V_{\text{los}} \geq 11000 \text{ km s}^{-1}$ , all with photometric  $V$ -band magnitudes ranging from 14.5 to 22. While our catalogue is devoid of all the foreground spectroscopic stars, we find a QSO<sup>4</sup> with 17.4  $V$ -band magnitude as well as 251 background galaxies in our catalogue as shown in Figure 6. Half of these spectroscopic background galaxies were catalogued as Coma cluster galaxy candidates in Godwin et al. (1983). Appendix A contains an extensive comparison of our structural parameters with the literature after removing all the known contaminants.

## 5 COLOUR-MAGNITUDE DIAGRAM

We show the colour-magnitude diagram (CMD) of all galaxies with detections in both  $V$  and  $R$ -bands in Figure 6. The  $V - R$  colours shown here (and used in all subsequent analyses) are from the SExtractor dual-image mode analysis described in Section 3. We measure the colours within matched apertures based on  $2.5 \times$  the Kron radius (Kron 1980) parameter determined from the  $R$ -band imaging rather than from the  $V$  and  $R$  total magnitudes. We note that these matched aperture colours are generally 0.2–0.3 mag redder than colours obtained from the total magnitudes. The black solid line, obtained from a linear fit to the bright ( $13 \leq V [\text{mag}] \leq 18$ ) and spectroscopically confirmed Coma cluster galaxies in our catalogue, highlights the red-sequence of galaxies. We extrapolate the red-sequence to fainter magnitudes and show in Figure 6 that the faint LSB galaxies from the Y16 are mostly consistent with the red-sequence, in agreement with a previous result from Koda et al. (2015). The  $1\sigma$  intrinsic scatter around the red-sequence was obtained in magnitude bins with width 2 mag and is shown as dashed lines in Figure 6. The scatter increases from  $\sim 0.06$  mag at  $V = 15$  mag to  $\sim 0.28$  mag for the faintest LSB galaxies. For subsequent analyses and discussion, we define three regions in our CMD: galaxies with colours within the limits defined by the  $1\sigma$  scatter around the best-fit line to red-sequence galaxies (RSG); galaxies with colours redder than the  $1\sigma$  limit ( $>\text{RSG}$ ), i.e. redder than the average RSG; and galaxies with colors bluer than the  $1\sigma$  limit ( $<\text{RSG}$ ), i.e. bluer than the average RSG.

In the context of cluster photometry, the red-sequence is normally expected to be populated by quiescent galaxies that are bound to the host cluster. However, our analysis in Section 4.4 shows that  $\sim 10$  per cent of the RSG with magnitudes brighter than  $V \sim 19$  mag do not belong to the Coma cluster. These bright background galaxies which have redshifts  $z \sim 0.2$  are known in the literature to be notoriously difficult to isolate with photometry only (Adami et al. 2006, 2009; Mahajan et al. 2011). As earlier mentioned, we have excluded these background galaxies from our catalogue and are left with 1,564 cluster galaxies with  $V < 19$  mag. At fainter apparent magnitudes, i.e.,  $19 \leq V [\text{mag}] \leq 22$ , spectroscopic background galaxies in the direction of the Coma cluster from the literature have elevated redshifts  $z \geq 0.3$  and are almost exclusively  $>\text{RSG}$ . A careful examination of these fainter background galaxies reveal that they generally have Sérsic index,  $n > 2$ . We assume that all other faint  $>\text{RSG}$  galaxies with  $n > 2$  are background galaxies and therefore exclude them from our catalogue. This brings the number

<sup>4</sup> This QSO is SDSS J125712.28+280543.3 at  $z = 1.29$  with  $V$ -band  $R_e \sim 5.4''$ .

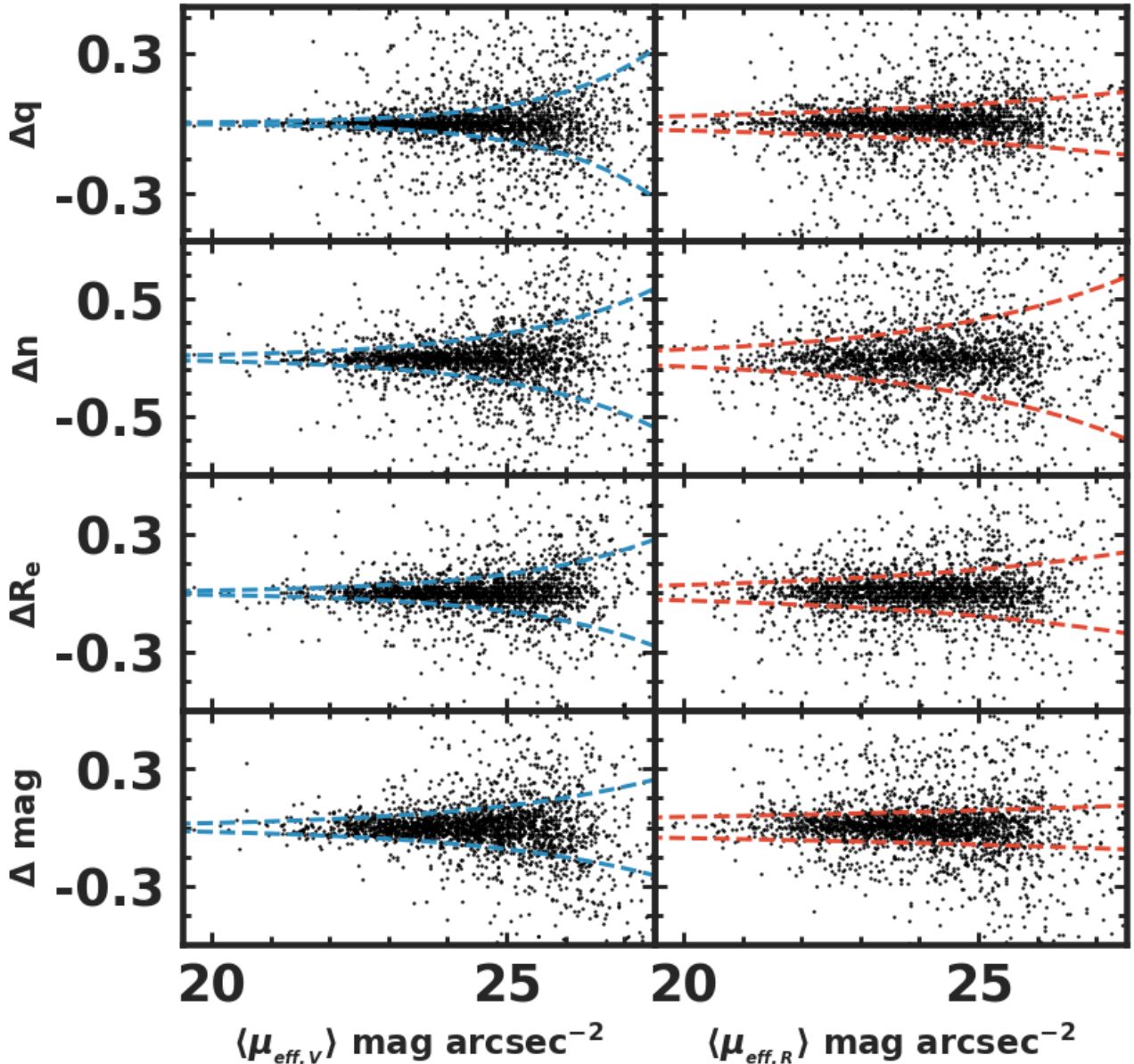


**Figure 5.** Variation of the structural parameters obtained from GALFIT modelling of galaxies with duplicate detections. We show on the x-axis  $V$  and  $R$ -band mean surface brightness within the effective radius (*left-hand panels* and *right-hand panels*, respectively) and on the y-axis, magnitude, effective radius, Sérsic index, and axial ratio. The dashed lines are fits to the 68th percentile of the corresponding ordinate parameter (in log) and are used to estimate the true model uncertainties as described in the text.

of remaining galaxies in our catalogue to 9, 179, with 64, 27, and 9 per cent being RSG, >RSG, and <RSG, respectively.

### 5.1 Control field

It should be noted that the spectroscopic sample used to isolate background galaxy contaminants is limited to high surface brightness galaxies, and as we have already shown, the red-sequence and surface brightness–magnitude diagnostics are both inadequate for weeding out all background galaxies. We therefore seek to know, statistically, the residual contamination level in our final catalogue. To this end, we analyse the  $V$  and  $R$  band observation of the Subaru Deep Field (SDF; Kashikawa et al. 2004) as a control field. The SDF is at a similar Galactic latitude as the Coma cluster and

was observed under similar photometric conditions (FWHM seeing  $\sim 0.98''$ ). It has similar field-of-view and limiting surface brightness as each of our Coma pointings, although it reaches a limiting magnitude that is  $\sim 1.5$  mag deeper than our Coma imaging data. Applying the same galaxy detection and quality control constraints (Sections 3 & 5) to the control field and assuming that it is representative of our Coma fields, we expect 2, 840 background galaxies within our combined Coma fields, mostly at fainter magnitudes, i.e.,  $V \sim 22$  mag, and redder colours, i.e.,  $V - R \sim 0.7$ , as shown in Figure 7.

Our control field analysis suggests that a minimum contamination level of  $\sim 0.02$  per cent is realised in our photometric catalogue below the red-sequence (<RSG). Along the red-sequence, i.e. in the RSG group, the residual contamination is  $\sim 20$  per cent, mostly

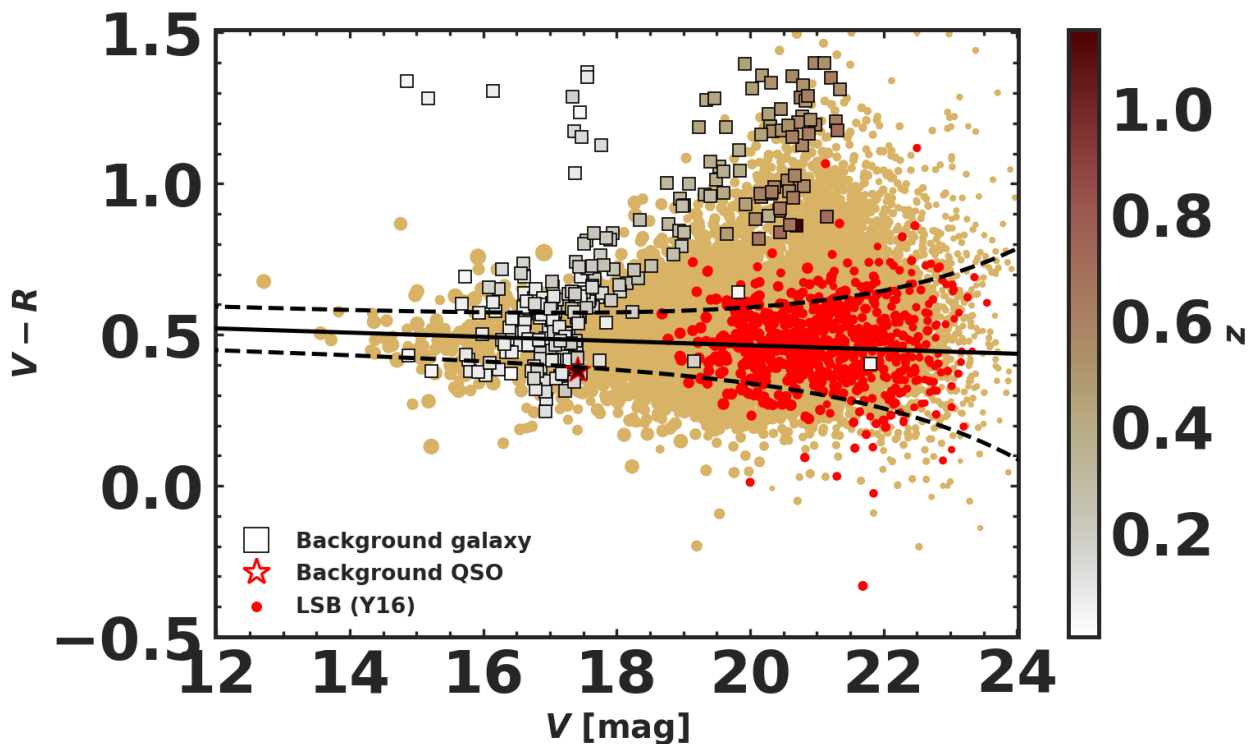


**Figure 6.** Colour–magnitude diagram of Coma cluster galaxies (brown circles) detected and analysed in this work. Galaxies from the low surface brightness catalogue of Y16, which mostly belong to the Coma cluster, are shown as red circles. Spectroscopically confirmed background galaxies in the direction of Coma cluster from the literature (filled squares) have been colour-coded by their redshifts. Also shown is a spectroscopically confirmed background quasi-stellar object (star marker with red edges, colour-coded by its redshift). We overlay the red-sequence (black solid line) obtained by a linear fit to the bright, spectroscopically confirmed cluster galaxies, extrapolated to faint magnitudes. We also show the  $1\sigma$  intrinsic scatter (black, dashed lines) around the red-sequence. The intrinsic scatter increases from  $\sim 0.06$  mag at  $V = 15$  mag to  $\sim 0.28$  mag for the faintest LSB galaxies. Most of the low surface brightness galaxies from Y16 have colours consistent with the red-sequence and fall within the limits of the  $1\sigma$  intrinsic scatter.

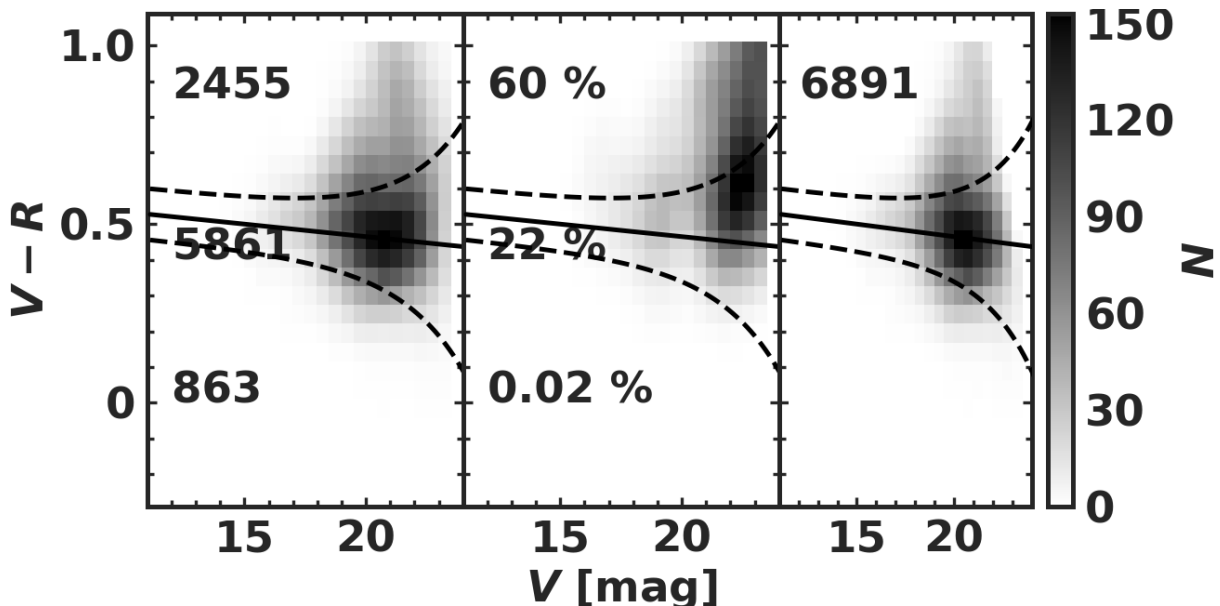


**Figure 7.** Histograms of colour–magnitude distribution of galaxies in the direction of the Coma cluster (*Left panel*), and in a control field – the Subaru Deep Field (*Middle Panel*), overlaid with the red-sequence of known Coma cluster galaxies. The solid and dashed black lines in all the panels are the same as in Figure 6. The background contaminants are mostly faint galaxies with  $V \sim 22.5$  mag and have very red colours  $V - R \sim 0.7$ . We summarize the number of galaxy candidates on and off the red-sequence in the left panel and the corresponding contamination levels in the middle panel. The *Right Panel* shows the colour–magnitude distribution of the remaining 6,891 Coma cluster galaxies after statistically correcting for the background contaminants. The colour-bar is the number density of the galaxies.

among the fainter ( $V > 19$  mag) LSB galaxies. Above the red-sequence ( $>$ RSG), the residual contamination level is very high, reaching  $\sim 60$  per cent. We summarize the residual contamination levels along and off the red-sequence in Figure 7 and note that the total number of Coma cluster galaxies in our catalogue drops to 6,891 galaxies after applying the statistical background-galaxy correction.

## 6 SUMMARY OF RESULTS

From our analysis thus far, we have obtained structural parameters (total magnitudes,  $R_e$ ,  $n$ ,  $q$ , and  $PA$  in both  $V$  and  $R$ -bands) in 9,179 galaxies in the direction of the Coma cluster. We show an example in Table 2 and make the complete catalogue available online. Due to the depth of our imaging data, we also identified 233 galaxies with faint, tidal features such as plumes, shells, rings, etc (see Figure 8). These features are the telltale signatures of the hierarchical nature of structure formation in the Universe. Table 2 contains a summary of galaxies with such tidal features.

As an example to highlight the wide range of galaxies in our catalogue, we show a  $120 \text{ kpc} \times 120 \text{ kpc}$  field near NGC 4911 in Figure 8. This field contains galaxies ranging from the giant spiral galaxy (NGC 4911) to the ultra-diffuse galaxy (Y48), as well as several dwarf galaxies. In addition, the field also contains a disrupting galaxy (COMA\_11\_4120), which as far as we know has not been previously catalogued in the literature.

Figure 9 shows the size–magnitude distribution of the Coma cluster galaxies. As expected, galaxy sizes correlate with their luminosities. In the  $V$ -band, we detect galaxies with mean surface brightness within the effective radius,  $\langle \mu_{\text{eff},V} \rangle$ , ranging from 20 to  $27.5 \text{ mag arcsec}^{-2}$ , effective radius,  $R_e$ , from  $\sim 0.6$  to  $\sim 15 \text{ kpc}$ , and apparent magnitudes from 12 to 24 mag. We therefore span a region of parameter space that contains a diversity of galaxies suitable for a systematic exploration of the Coma cluster. As shown in both panels of Figure 9, our catalogue contains a large sample of low surface brightness galaxies ( $\langle \mu_{\text{eff},V} \rangle \geq 24 \text{ mag arcsec}^{-2}$ ) with small sizes ( $R_e \leq 1 \text{ kpc}$ ) structurally similar to some Local Group dwarf galaxies. Our catalogue also contains galaxies with intermediate surface brightness  $22 \leq \langle \mu_{\text{eff},V} \rangle \leq 24.5$  and  $R_e \geq 2.5 \text{ kpc}$ , a region of the parameter space relatively unexplored and often misunderstood as being devoid of galaxies (compare our Figure 9 with fig. 4 from Koda et al. 2015). This confirms the previous result from the Danieli & van Dokkum (2019) where they also reported that this region is filled although their sample is incomplete below  $\sim 2 \text{ kpc}$ .

We split our final catalogue into high surface brightness (HSB), intermediate surface brightness (ISB), and LSB galaxies using the following mean surface brightness limits – HSB:  $\langle \mu_{\text{eff},V} \rangle < 23 \text{ mag arcsec}^{-2}$ ; ISB:  $23 \geq \langle \mu_{\text{eff},V} \rangle < 24.5 \text{ mag arcsec}^{-2}$ ; and LSB:  $\langle \mu_{\text{eff},V} \rangle \geq 24.5 \text{ mag arcsec}^{-2}$ . These limits, which are in line with the categorization scheme used in Martin et al. (2019), are simply for convenience and we do not ascribe any particular astrophysical meaning to them. The bright limit of the LSB category is consistent with the LSB limit used in Y16 catalogue. Our catalogue contains 2,290 HSB, 3,833 ISB, and 3,056 LSB galaxies as defined above. This implies a factor of 3 increase in the number of LSB galaxies in the Coma cluster relative to the Y16 catalogue after accounting for background galaxy contamination. We show the distributions of the structural parameters in the 3 surface brightness categories in Figure 10 and note that regardless of surface brightness, the most likely galaxy in our catalogue has  $V$ -band magnitude  $\sim 21$  mag,  $R_e \sim 0.8 \text{ kpc}$ ,  $n \sim 1$ ,  $q \sim 0.8$ , and is most likely aligned

along the  $PA$  of the cluster, i.e.  $\sim 71$  deg (Plionis 1994). The second subpanel shows that there is no obvious discontinuity in the sizes of the LSB galaxy subpopulation at  $1.5 \text{ kpc}$  that would mark UDGs as a distinct galaxy population.

Lastly, we note that Forbes et al. (2020) used  $V - R$  colours from this work, which were based on the difference between the total  $V$  and total  $R$  magnitudes, to explore the possible trends of globular cluster specific frequency with host UDG colour. Here, we have used a different approach to calculate the  $V - R$  colours of UDGs using colours from matched apertures as discussed in Section 5. This results in a similar specific frequency vs UDG colour trend to that found by Forbes et al. (2020).

### 6.1 New ultra-diffuse galaxies in the Coma cluster

Having established that our catalogue is rich in LSB galaxies, we immediately conduct a further search for new ultra-diffuse galaxies within the outlined UDG region shown in Figure 9. This region contains 110 galaxies after excluding all the UDGs already identified in the literature, but only 29 satisfy all the commonly used UDG criteria, i.e.  $R_e \geq 1.5 \text{ kpc}$ ; mean surface brightness within  $R_e$ ,  $\langle \mu_{\text{eff},V} \rangle \geq 24.5 \text{ mag arcsec}^{-2}$  (combining criterion 6 from Y16 and using the mean UDG colour  $V - R \sim 0.5$ ); and  $\langle \mu_{\text{eff},V} \rangle - \mu_{\text{eff},V} \leq 0.8$  (see criterion 7 in Y16) where  $\mu_{\text{eff},V}$  is the surface brightness at  $R_e$ . We note that this last condition limits the sample of acceptable UDGs to those with Sérsic index,  $n \leq 1.25$ , i.e. exponential light profiles. Two factors may be responsible for these new detections: our data while covering the same sky area as that used in Y16 had better seeing, and we have applied the detection methods originally introduced in Y16 to multi-band data, making our measurements more reliable. We show these newly discovered UDGs in Figure 11 and present their structural parameters in Table 3. Out of these newly catalogued UDGs, 23 lie along the red-sequence of Coma cluster galaxies, i.e. they are RSG as discussed in Section 5, with the remaining 2 having colours redder than the red-sequence region.

### 6.2 Environmental trends in clustercentric colour distribution

We now revisit the issue of environmental colour trends in the Coma cluster with emphasis on the LSB galaxies in our photometric catalogue. To recap, our catalogue contains 3,056 LSB galaxies, most of which are along the red-sequence with 154 and 631 galaxies bluer and redder than the red-sequence region of the colour–magnitude diagram, respectively, as defined in Section 5. Our control field analysis in Section 5.1 already shows that we can expect very little background galaxy contamination in the subsample that is bluer than the red-sequence, and up to  $\sim 60$  per cent contamination in the LSB galaxy subsample that is redder than the red-sequence. Along the red-sequence, the maximum background galaxy contamination level is  $\sim 20$  per cent.

Galaxy clusters such as Coma are well known to show a decreasing colour gradient with projected clustercentric distance (Terlevich et al. 2001), which is believed to be directly linked to a corresponding age gradient (Smith et al. 2009; Smith et al. 2011). The densest region of the cluster is observed to be dominated by redder galaxies while bluer galaxies dominate the less dense outskirts regions. Within the Coma cluster, the correlation of galaxy colours with their local environment has been previously observed in dwarf galaxies (Secker et al. 1997), although Adami et al. (2006)



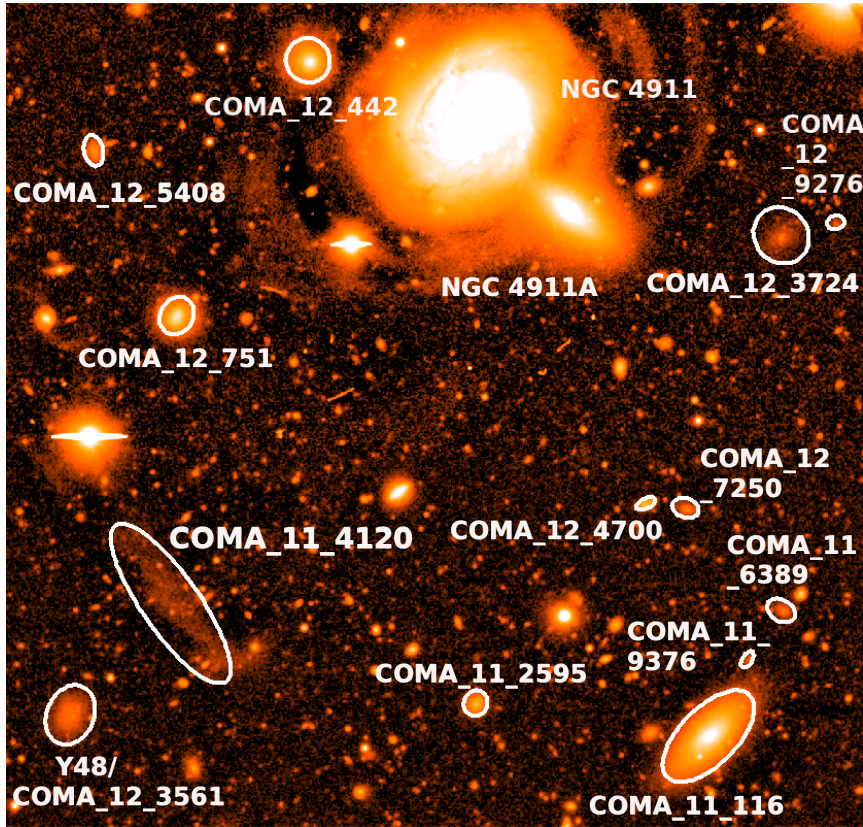


**Figure 8.** An example of the wide range of galaxies with structural parameters present in our final catalogue. We show the V-band Subaru/Suprime-Cam imaging of a field at  $\sim 0.6$  Mpc from the centre of the Coma cluster with dimensions  $120 \text{ kpc} \times 120 \text{ kpc}$ . The galaxies in our final catalogue are marked with white  $1R_e$  isophotes. This field contains the giant spiral galaxy, NGC 4911, several dwarf galaxies, and the ultra-diffuse galaxy, Y48 (COMA.12.3561). It also includes a faint, disrupting galaxy (COMA.11.4120) that is  $\sim 75$  kpc away from the NGC 4911–NGC 4911A interacting pair. North is up and East is left.

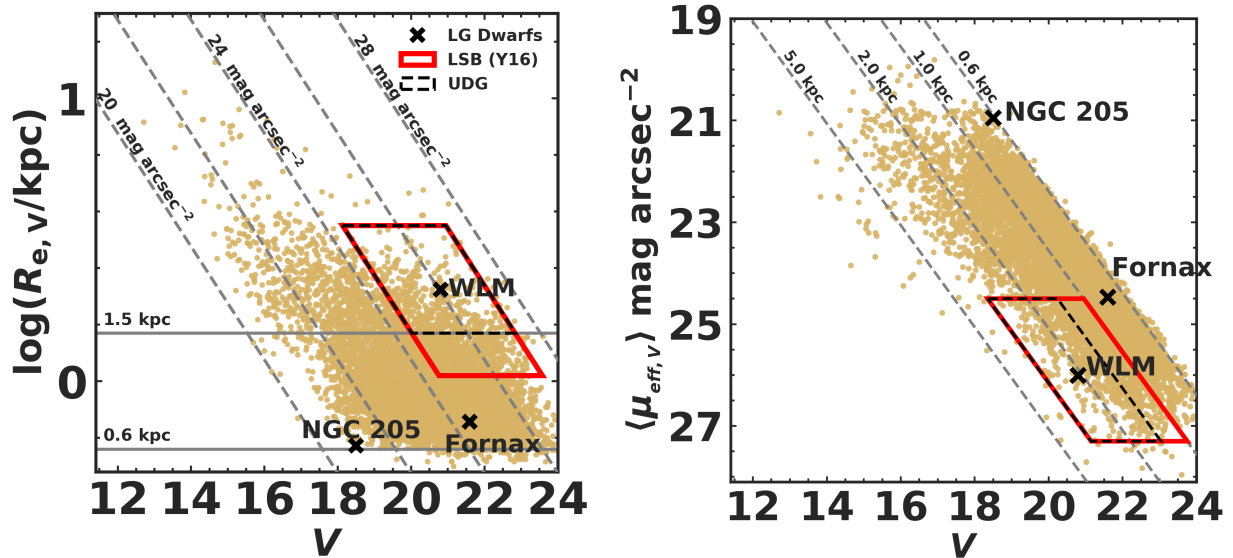


**Figure 9.** *Left panel:* Size–magnitude distribution of Coma cluster galaxies. The brown circles are the 9,179 galaxies successfully modeled with a single Sérsic function as described in the text. The dashed lines correspond to constant mean effective surface brightness. We detect Coma cluster galaxies as small as  $\sim 0.6$  kpc and with mean surface brightness within the effective radius as faint as  $\sim 27.5 \text{ mag arcsec}^{-2}$ . For context, we show the regions where the low surface brightness galaxies in the catalogue of Yagi et al. (2016) may be found (red parallelogram), as well as that of the ultra-diffuse galaxies (black, dashed parallelogram). We also show and label some Local Group dwarf galaxies (black crosses) from the compilation of McConnachie (2012) that would fall within our detection limits, assuming they were observed at the distance of the Coma cluster. These are the dwarf irregular galaxy Wolf-Lundmark-Melotte (WLM), the Fornax dwarf spheroidal galaxy and the dwarf elliptical galaxy NGC 205. *Right panel:* Mean surface brightness within the effective radius of Coma cluster galaxies versus their V-band apparent magnitudes. The dashed lines correspond to constant effective radius. The outlines and the black crosses are the same as shown in the left panel.

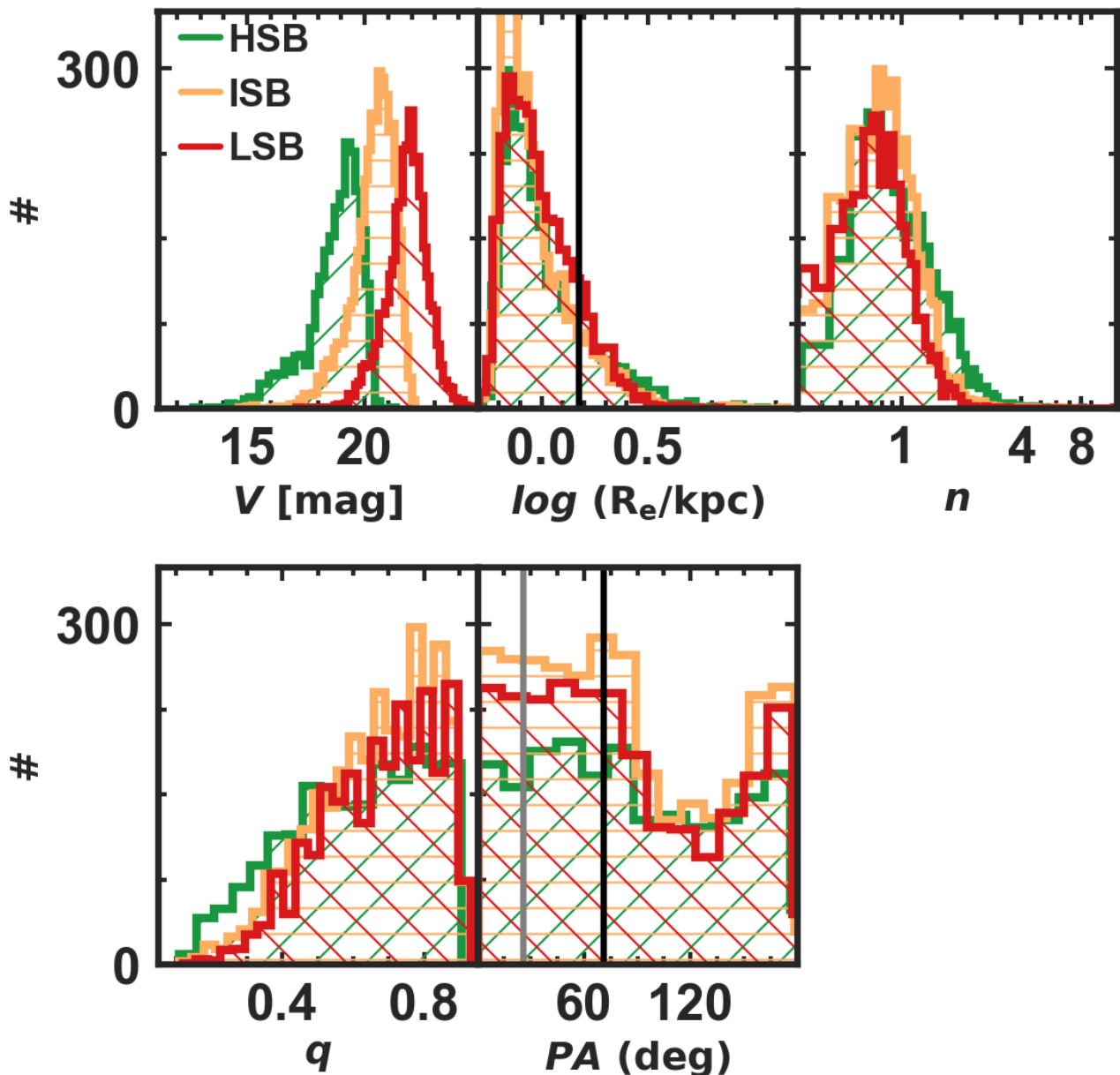


**Figure 10.** Distribution of the structural parameters from  $V$ -band GALFIT analysis of Coma cluster galaxies in bins of high (HSB), intermediate (ISB), and low (LSB) mean surface brightness, as defined in the text. *Top panels* show the distributions of the  $V$ -band magnitudes, physical sizes, Sérsic indices while the *bottom panels* show the axial ratios and the folded position angles of Coma cluster galaxies, respectively. Within the size and surface brightness limits of our catalogue, the most likely Coma cluster galaxy has  $V \sim 21$  mag,  $R_e \sim 0.8$  kpc,  $n \sim 1$ , and  $q \sim 0.8$ . The solid vertical line in the second subpanel is the fiducial size limit for UDGs. There is no obvious discontinuity at this size limit that would mark UDGs as a distinct galaxy subpopulation. In the position angle subpanel, we have highlighted the major-axis of the cluster with the black line and also show the  $PA$  of NGC 4874, the central cD galaxy, with the gray line. We note that there is a remarkable drop in the number of galaxies with  $PA \sim 120^\circ$  in all surface brightness bins.

reported no radial trends in their sample of faint LSB galaxies. [Alabi et al. \(2018\)](#), however, found hints that UDGs within the cluster core may be redder than those in the cluster outskirts, although the analysis was severely limited by incomplete and inhomogeneously sourced colour data. More generally, LSB galaxies are expected to have formed their stars rapidly at earlier epochs ([Martin et al. 2019](#)) while those observed in dense environments may have experienced enhanced star-formation quenching via ram-pressure stripping and tidal puffing-up effects from their host clusters ([Moore et al. 1996](#); [Johansson et al. 2009](#)). Imprints of such physical pro-

cesses are expected to be seen in the radial distribution of the galaxy colours ([Jiang et al. 2019](#)). [Sales et al. \(2020\)](#) recently used the IllustrisTNG cosmological simulations to show that UDGs that were accreted early into present-day massive clusters ( $\sim 10^{14} M_\odot$ ) are found mostly within the cluster cores while those accreted more recently from the field environments dominate in the cluster outskirts.

Figure 12 shows how the mean residual  $V - R$  colour distribution with respect to the best-fit red-sequence line varies with projected clustercentric radii out to the cluster virial radius, i.e.

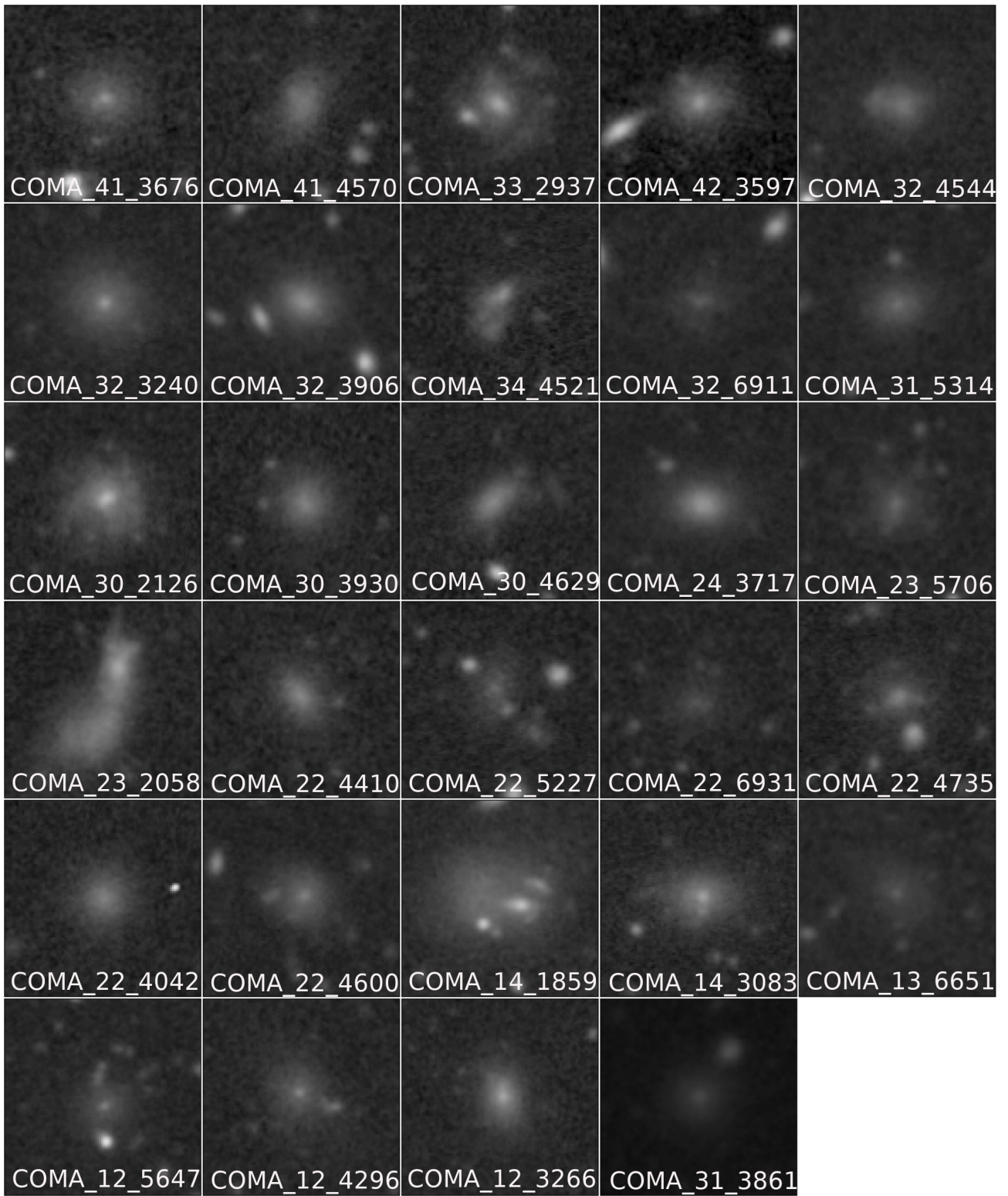


**Figure 11.** V-band Subaru/Suprime-Cam thumbnails of the 29 newly discovered Coma cluster ultra-diffuse galaxies. These UDGs have a typical  $R_e \sim 2$  kpc and  $\langle \mu_{\text{eff},V} \rangle \sim 25$  mag arcsec $^{-2}$ . Each thumbnail is  $10 \times 10$  kpc across. North is up and East is to the left.

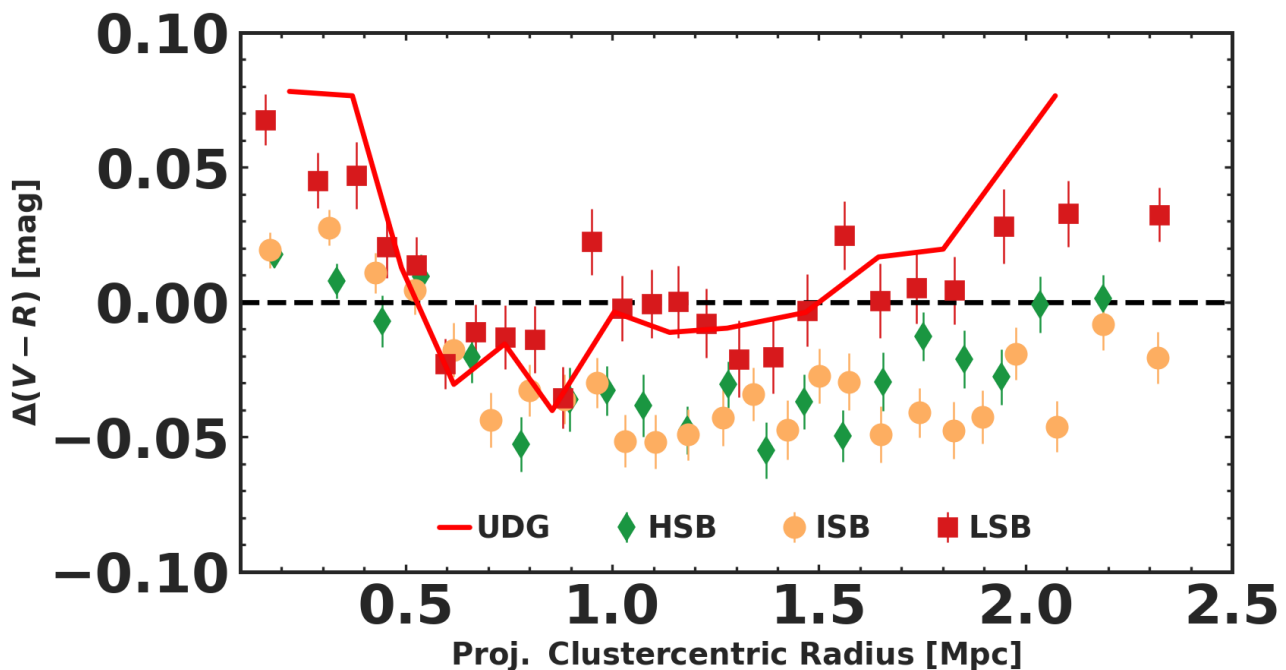


**Figure 12.** Mean residual  $V - R$  colours of Coma cluster galaxies after subtracting off the global red-sequence fit versus the projected clustercentric radius. We show results for the high (HSB), intermediate (ISB), and low (LSB) surface brightness galaxies, using the limits discussed in the text. Ultra-diffuse galaxies (UDG) which are represented by the solid red line have similar mean residual colour trends as the LSB galaxies out to the virial radius of the Coma cluster ( $\sim 2.9$  Mpc). We do not include galaxies that are redder than the  $1\sigma$  scatter around the best-fit red-sequence line in this plot due to their high background contamination rate. The dashed horizontal line corresponds to galaxies with mean colours consistent with the red-sequence and it is shown to guide the eye. LSB galaxies within the cluster core have redder mean residual colours relative to the red-sequence relation at the  $2\sigma$  level and they show a more dramatic transition at  $\sim 0.6$  Mpc compared to galaxies with higher surface brightness, beyond which their mean residual colour flattens out, before rising in the cluster outskirts.

$\sim 2.9$  Mpc (Kubo et al. 2007). We have excluded all galaxies that are redder than the  $1\sigma$  scatter around the best-fit line of the red-sequence without spectroscopic confirmation as Coma cluster members in estimating the mean colour residuals. This is due to their high background galaxy contamination rate. Relative to the red-sequence, LSB galaxies (and UDGs) have redder mean colours compared to ISB and HSB galaxies within the cluster core. They have a mean residual colour that is  $0.034 \pm 0.014$  mag redder compared to higher surface brightness galaxies. This result, which is significant at the  $2\sigma$  level, suggests that LSB galaxies are most vulnerable to the severe star-formation quenching effects of the cluster-core environment. Outside the cluster-core, the mean residual colour trends are similar out to  $\sim 1.8$  Mpc for the various surface brightness subsamples. The high mean residual colour at larger projected clustercentric radii, which is more evident in the LSB galaxies, can be attributed to an increase in the contribution from the redder, fainter background contamination galaxies to our final catalogue (see Section 5.1).

There is a noticeable transition at  $\sim 0.6$  Mpc ( $\sim 0.3R_{200}$ ), which is more pronounced in the LSB galaxies, already hinted at in Alabi et al. (2018). This transition radius corresponds to the projected radius within which UDGs that formed from cluster tidal effects dominate the UDG clustercentric number density profile in the cosmological simulations of Sales et al. (2020, see their fig. 7). The observed transition radius ( $\sim 0.6$  Mpc) is similar to the the projected scale radius ( $r_s \sim 27'$  or  $\sim 0.8$  Mpc at the distance of the Coma cluster) of the Coma cluster dark matter halo (Okabe et al. 2014). Similar transition radii have been observed in the Virgo cluster (Chung et al. 2009) and more recently in galaxy clusters in the SAMI

Galaxy Survey (Owers et al. 2019). In both studies, the transition radius, although inferred from different parameters, was linked to environmental quenching effects which is most pronounced in the the cluster cores. For example, spiral galaxies within  $\sim 0.5$  Mpc ( $\sim 0.3R_{200}$ ) from the centre of Virgo cluster have HI disks that are smaller than their stellar disks, while in the SAMI Galaxy Survey, galaxies with strong Balmer absorption features but no recent star-formation episodes, were found exclusively within  $\sim 0.6R_{200}$  of the cluster centres.

## 7 CONCLUSION

In this work, we have obtained structural parameters simultaneously in  $V$  and  $R$ -bands for 9, 179 galaxies within an area of  $\sim 4$  deg $^2$  in the Coma cluster using Subaru/Subprime-Cam data. Importantly, we have coherently obtained the  $V - R$  colours of the ultra-diffuse galaxies in the Coma cluster, and in the more general class of low surface brightness galaxies, out to  $\sim 2.6$  Mpc from the centre of the cluster. Our catalogue contains galaxies with magnitudes as faint as  $V \sim 24$  mag, effective radius,  $R_e$ , as small as  $\sim 0.6$  kpc, and mean effective surface brightness within effective radius,  $\langle \mu_{\text{eff},V} \rangle$ , as low as  $\sim 27.5$  mag arcsec $^{-2}$ .

Our catalogue contains an unprecedented 3, 056 LSB galaxies in the direction of Coma cluster with mean effective surface brightness fainter than 24 mag arcsec $^{-2}$  in the  $V$ -band. Out of these Coma cluster LSB galaxies, we found 29 new UDGs, previously uncatalogued in the literature. In addition, we identified galaxies with faint tidal features within the Coma cluster. We make this cat-



atalogue publicly available. We have confirmed earlier results that most Coma cluster UDGs lie along the red-sequence of the colour-magnitude relation, but we found subpopulations of UDGs outside the red-sequence region.

We also investigated clustercentric trends in galaxy colours in order to understand how the locally varying environment within the cluster affects the LSB galaxies compared to co-spatial higher surface brightness galaxies within the Coma cluster. We obtained the important result of a cluster transition radius at projected radius  $\sim 0.6$  Mpc, within which the LSB galaxies are on average redder than galaxies with higher surface brightnesses at the  $2\sigma$  level. This transition radius is similar to the region reported by Sales et al. (2020) based on the IllustrisTNG cosmological simulation of massive clusters of galaxies within which ancient infalls dominate the UDG population.

## ACKNOWLEDGEMENTS

We thank the anonymous referee for the thoughtful reading of the manuscript and for the valuable feedback. DAF thanks the ARC for financial support via DP160101608. JPB and AJR acknowledge financial support from AST-1616598, AST-1518294 and AST-1616710. AJR was supported by the Research Corporation for Science Advancement as a Cottrell Scholar. This paper was based in part on data collected at the Subaru Telescope, which is operated by the National Astronomical Observatory of Japan. This research made use of the “K-corrections calculator” service available at <http://kcor.sai.msu.ru/>, TOPCAT software available at <http://www.starlink.ac.uk/topcat/> (Taylor 2005), and SEP software (Barbary 2016).

## DATA AVAILABILITY

The data underlying this article are available in the article and in its online supplementary material.

## REFERENCES

- Abraham R. G., van Dokkum P. G., 2014, *PASP*, **126**, 55  
 Adami C., et al., 2006, *A&A*, **459**, 679  
 Adami C., et al., 2009, *A&A*, **507**, 1225  
 Aguerri J. A. L., Iglesias-Páramo J., Vilchez J. M., Muñoz-Tuñón C., Sánchez-Janssen R., 2005, *AJ*, **130**, 475  
 Ahn C. P., et al., 2012, *ApJS*, **203**, 21  
 Alabi A., et al., 2018, *MNRAS*, **479**, 3308  
 Barbary K., 2016, *The Journal of Open Source Software*, **1**, 58  
 Bertin E., Arnouts S., 1996, *A&AS*, **117**, 393  
 Blanton M. R., Roweis S., 2007, *AJ*, **133**, 734  
 Carter D., et al., 2002, *ApJ*, **567**, 772  
 Carter D., et al., 2008, *ApJS*, **176**, 424  
 Chiboucas K., Tully R. B., Marzke R. O., Trentham N., Ferguson H. C., Hammer D., Carter D., Khosroshahi H., 2010, *ApJ*, **723**, 251  
 Chilingarian I. V., Zolotukhin I. Y., 2012, *MNRAS*, **419**, 1727  
 Chilingarian I. V., Melchior A.-L., Zolotukhin I. Y., 2010, *MNRAS*, **405**, 1409  
 Chilingarian I. V., Afanasiev A. V., Grishin K. A., Fabricant D., Moran S., 2019, *The Astrophysical Journal*, **884**, 79  
 Chung A., van Gorkom J. H., Kenney J. D. P., Crowl H., Vollmer B., 2009, *The Astronomical Journal*, **138**, 1741  
 Danieli S., van Dokkum P., 2019, *ApJ*, **875**, 155  
 Edwards S. A., Colless M., Bridges T. J., Carter D., Mobasher B., Poggianti B. M., 2002, *ApJ*, **567**, 178  
 Eisenhardt P. R., Propris R. D., Gonzalez A. H., Stanford S. A., Wang M., Dickinson M., 2007, *The Astrophysical Journal Supplement Series*, **169**, 225  
 Ferré-Mateu A., et al., 2018, *MNRAS*, **479**, 4891  
 Forbes D. A., Alabi A., Romanowsky A. J., Brodie J. P., Arimoto N., 2020, *MNRAS*, **492**, 4874  
 Godwin J. G., Metcalfe N., Peach J. V., 1983, *MNRAS*, **202**, 113  
 Graham A. W., Driver S. P., 2005, *PASA*, **22**, 118  
 Gutiérrez C. M., Trujillo I., Aguerri J. A. L., Graham A. W., Caon N., 2004, *ApJ*, **602**, 664  
 Häussler B., et al., 2007, *ApJS*, **172**, 615  
 Hoyos C., et al., 2011, *MNRAS*, **411**, 2439  
 Jiang F., Dekel A., Freundlich J., Romanowsky A. J., Dutton A. A., Macciò A. V., Di Cintio A., 2019, *MNRAS*, **487**, 5272  
 Johansson P. H., Naab T., Ostriker J. P., 2009, *ApJ*, **697**, L38  
 Kadowaki J., Zaritsky D., Donnerstein R. L., 2017, *ApJ*, **838**, L21  
 Kashikawa N., et al., 2004, *PASJ*, **56**, 1011  
 Kelly P. L., et al., 2014, *MNRAS*, **439**, 28  
 Koda J., Yagi M., Yamanoi H., Komiyama Y., 2015, *ApJ*, **807**, L2

ID	RA [Degree]	Dec [Degree]	$V$ [mag]	$R_{\text{eff}}$ [kpc]	$\langle \mu_{\text{eff}} \rangle$ [mag arcsec $^{-2}$ ]	$n_V$	$q_V$	$PA_V$ [deg]	$R$ [mag]	$R_{\text{eff}}$ [kpc]	$\langle \mu_{\text{eff}} \rangle$ [mag arcsec $^{-2}$ ]	$n_R$	$q_R$	$PA_R$ [deg]	$V-R$ [mag]	comment
(1)	(2)	(3)	(4)	(5)	(6)	(7)	(8)	(9)	(10)	(11)	(12)	(13)	(14)	(15)	(16)	(17)
COMA-10.1339	195.41327	27.160273	18.81 ± 0.21	4.31 ± 0.3	25.55 ± 0.26	11.7 ± 50.62	0.89 ± 0.14	80.79	18.41 ± 0.23	5.87 ± 0.4	25.81 ± 0.27	13.42 ± 0.69	0.88 ± 0.14	80.58	0.81	LSB, > RS, GMP1928
COMA-10.2134	195.34398	26.830603	19.36 ± 0.18	2.64 ± 0.22	25.04 ± 0.25	1.02 ± 0.51	0.7 ± 0.14	146.28	18.7 ± 0.19	2.3 ± 0.19	24.08 ± 0.24	0.43 ± 0.55	0.49 ± 0.12	141.41	0.71	LSB, Y16
COMA-10.2157	195.24165	26.97631	19.37 ± 0.22	3.43 ± 0.24	25.62 ± 0.27	0.62 ± 0.58	0.56 ± 0.15	147.71	18.43 ± 0.19	3.74 ± 0.23	24.86 ± 0.23	0.66 ± 0.59	0.6 ± 0.13	148.88	0.71	LSB, Y11, DF44
COMA-10.2222	195.31602	27.210728	19.41 ± 0.2	2.93 ± 0.23	25.31 ± 0.26	0.76 ± 0.54	0.57 ± 0.14	9.26	18.58 ± 0.17	3.05 ± 0.21	24.57 ± 0.23	0.77 ± 0.58	0.6 ± 0.13	9.08	0.62	LSB, Y13, DFX1, GMP2175
COMA-10.3142	195.19983	27.00997	19.9 ± 0.16	1.77 ± 0.21	24.71 ± 0.3	1.6 ± 0.48	0.84 ± 0.13	111.51	19.69 ± 0.21	1.91 ± 0.22	24.66 ± 0.3	1.4 ± 0.58	1.0 ± 0.13	20.13	0.38	LSB
COMA-10.3630	195.32954	27.054224	20.11 ± 0.25	2.92 ± 0.26	26.0 ± 0.31	0.82 ± 0.63	0.73 ± 0.15	16.89	19.69 ± 0.18	2.61 ± 0.25	25.35 ± 0.3	0.82 ± 0.61	0.87 ± 0.13	178.5	0.73	LSB, Y14, DF42
COMA-10.4551	195.27219	27.15981	20.51 ± 0.17	1.42 ± 0.21	24.85 ± 0.37	0.78 ± 0.49	0.8 ± 0.13	149.52	19.75 ± 0.16	1.43 ± 0.19	24.1 ± 0.33	0.81 ± 0.56	0.8 ± 0.12	145.8	0.6	LSB, Y12
COMA-10.4682	195.27608	27.16667	20.57 ± 0.18	1.51 ± 0.22	25.03 ± 0.36	1.01 ± 0.51	0.97 ± 0.14	0.6	19.81 ± 0.17	1.52 ± 0.2	24.29 ± 0.33	0.98 ± 0.13	0.98 ± 0.13	53.72	0.55	LSB, Y18
COMA-10.5089	195.197	26.78314	20.73 ± 0.27	2.48 ± 0.27	26.26 ± 0.36	0.73 ± 0.67	0.66 ± 0.16	141.95	20.07 ± 0.22	2.39 ± 0.27	25.53 ± 0.32	0.71 ± 0.62	0.64 ± 0.14	140.62	0.47	LSB, Y8, DF46
COMA-10.5457	195.18846	27.113832	20.87 ± 0.2	1.53 ± 0.23	25.36 ± 0.39	0.99 ± 0.55	0.89 ± 0.14	112.1	20.2 ± 0.18	1.47 ± 0.21	24.6 ± 0.36	0.9 ± 0.58	0.83 ± 0.13	114.37	0.46	LSB, Y6
COMA-10.5633	195.5619	27.14568	20.94 ± 0.32	2.75 ± 0.3	26.7 ± 0.4	1.6 ± 0.74	0.69 ± 0.17	54.99	20.25 ± 0.22	2.39 ± 0.28	25.71 ± 0.34	1.21 ± 0.63	0.77 ± 0.14	59.63	0.58	LSB, Y22
COMA-10.5695	195.40529	27.006954	20.97 ± 0.18	1.27 ± 0.22	25.06 ± 0.42	1.84 ± 0.52	0.79 ± 0.14	21.01	20.96 ± 0.2	1.29 ± 0.24	25.08 ± 0.45	1.43 ± 0.6	0.82 ± 0.13	25.41	0.38	LSB
COMA-10.5842	195.53276	26.87714	21.03 ± 0.16	1.07 ± 0.21	24.75 ± 0.46	1.0 ± 0.48	0.84 ± 0.13	70.96	20.93 ± 0.18	1.04 ± 0.21	24.59 ± 0.48	0.99 ± 0.58	0.85 ± 0.13	70.04	0.41	LSB
COMA-10.5902	195.27608	27.168835	21.05 ± 0.16	1.04 ± 0.21	24.7 ± 0.47	1.56 ± 0.47	0.96 ± 0.13	44.88	20.82 ± 0.17	0.99 ± 0.2	24.37 ± 0.47	1.52 ± 0.54	0.73 ± 0.13	102.32	0.51	LSB, > RS
COMA-10.6090	195.30705	26.866377	21.12 ± 0.15	0.92 ± 0.2	24.51 ± 0.5	0.27 ± 0.46	0.52 ± 0.13	123.13	20.33 ± 0.14	0.9 ± 0.17	23.66 ± 0.43	0.61 ± 0.54	0.89 ± 0.12	101.31	0.94	LSB, > RS
COMA-10.6392	195.49966	26.873947	21.24 ± 0.16	0.94 ± 0.21	24.67 ± 0.51	0.89 ± 0.47	0.87 ± 0.13	8.58	20.89 ± 0.17	0.94 ± 0.2	24.31 ± 0.49	0.9 ± 0.56	0.92 ± 0.13	39.74	0.59	LSB
COMA-10.6422	195.42538	26.661331	21.25 ± 0.15	0.88 ± 0.2	24.55 ± 0.53	1.03 ± 0.46	0.79 ± 0.13	3.59	21.1 ± 0.17	1.78 ± 0.25	24.27 ± 0.54	1.06 ± 0.56	0.81 ± 0.13	18.33	0.41	LSB
COMA-10.6462	195.58606	27.102407	21.26 ± 0.25	1.7 ± 0.26	25.98 ± 0.41	0.79 ± 0.63	0.46 ± 0.15	14.57	20.42 ± 0.2	1.78 ± 0.25	25.24 ± 0.36	0.76 ± 0.61	0.5 ± 0.13	11.53	0.62	LSB, Y24
COMA-10.6536	195.48225	27.10293	21.29 ± 0.15	0.86 ± 0.2	24.54 ± 0.54	0.47 ± 0.46	0.8 ± 0.13	174.8	20.93 ± 0.16	0.85 ± 0.19	24.15 ± 0.51	0.72 ± 0.56	0.89 ± 0.13	5.25	0.59	LSB
COMA-10.6577	195.130359	26.793341	21.31 ± 0.16	0.96 ± 0.21	24.77 ± 0.51	0.79 ± 0.48	0.43 ± 0.13	20.89	20.76 ± 0.16	0.93 ± 0.19	24.16 ± 0.47	1.02 ± 0.56	0.45 ± 0.13	17.05	0.8	LSB, > RS
COMA-10.6622	195.5833	27.209324	21.32 ± 0.23	1.52 ± 0.25	25.8 ± 0.43	0.58 ± 0.61	0.72 ± 0.15	57.73	20.57 ± 0.19	1.48 ± 0.23	24.99 ± 0.39	0.57 ± 0.6	0.75 ± 0.13	55.81	0.6	LSB, Y25
COMA-10.6670	195.3495	26.75686	21.34 ± 0.23	1.47 ± 0.25	25.73 ± 0.43	0.83 ± 0.6	0.67 ± 0.15	28.37	20.62 ± 0.19	1.47 ± 0.24	25.02 ± 0.4	0.83 ± 0.6	0.73 ± 0.13	27.93	0.47	LSB, Y15
COMA-10.6731	195.36357	26.667072	21.38 ± 0.22	1.41 ± 0.25	25.69 ± 0.44	0.38 ± 0.59	0.58 ± 0.15	26.1	21.24 ± 0.21	1.3 ± 0.26	25.38 ± 0.48	0.45 ± 0.62	0.67 ± 0.13	29.89	0.48	LSB
COMA-10.6914	195.12947	27.020304	21.45 ± 0.29	1.93 ± 0.28	26.43 ± 0.43	0.64 ± 0.7	0.75 ± 0.16	155.83	20.73 ± 0.23	2.0 ± 0.28	25.8 ± 0.38	0.81 ± 0.64	1.0 ± 0.14	152.38	0.58	LSB, Y3
COMA-10.7073	195.24005	26.781855	21.52 ± 0.19	1.1 ± 0.23	25.29 ± 0.49	0.5 ± 0.54	0.73 ± 0.14	80.52	21.2 ± 0.18	1.0 ± 0.22	24.76 ± 0.51	0.68 ± 0.59	0.76 ± 0.13	75.55	0.53	LSB
COMA-10.7100	195.54	27.135769	21.53 ± 0.19	1.04 ± 0.23	25.2 ± 0.51	0.82 ± 0.53	0.66 ± 0.14	60.87	21.26 ± 0.19	1.04 ± 0.23	24.91 ± 0.51	0.9 ± 0.59	0.62 ± 0.13	58.82	0.53	LSB
COMA-10.7154	195.144787	27.162666	21.55 ± 0.17	0.91 ± 0.22	24.9 ± 0.54	0.88 ± 0.5	0.89 ± 0.14	146.76	21.42 ± 0.18	0.83 ± 0.21	24.57 ± 0.58	1.02 ± 0.58	0.66 ± 0.13	113.28	0.41	LSB
COMA-10.7270	195.57613	26.69556	21.59 ± 0.27	1.62 ± 0.27	26.21 ± 0.45	0.22 ± 0.67	0.69 ± 0.16	64.54	20.97 ± 0.22	1.68 ± 0.27	25.67 ± 0.42	0.17 ± 0.63	0.75 ± 0.14	65.6	0.4	LSB, Y23
COMA-10.7279	195.244732	27.152234	21.61 ± 0.16	0.8 ± 0.21	24.68 ± 0.59	0.3 ± 0.47	0.64 ± 0.13	76.16	20.98 ± 0.15	0.76 ± 0.18	23.95 ± 0.54	0.38 ± 0.53	0.66 ± 0.12	75.74	0.93	LSB, > RS
COMA-10.7296	195.54225	26.934872	21.61 ± 0.19	1.02 ± 0.23	25.23 ± 0.52	0.95 ± 0.54	0.91 ± 0.14	39.0	21.22 ± 0.19	1.1 ± 0.23	25.0 ± 0.5	1.05 ± 0.6	0.93 ± 0.13	54.9	0.63	LSB, > RS
COMA-10.7296	195.25078	26.677841	21.62 ± 0.17	0.9 ± 0.22	24.96 ± 0.56	1.17 ± 0.5	0.53 ± 0.14	6.42	20.97 ± 0.16	0.86 ± 0.19	24.22 ± 0.52	1.4 ± 0.56	0.53 ± 0.13	7.34	0.85	LSB, > RS
COMA-10.7323	195.48868	26.91578	21.63 ± 0.15	0.76 ± 0.2	24.59 ± 0.61	0.96 ± 0.46	0.85 ± 0.13	57.95	21.24 ± 0.16	0.7 ± 0.19	24.03 ± 0.6	1.0 ± 0.55	0.87 ± 0.12	59.36	0.62	LSB
COMA-10.7374	195.10555	27.184435	21.65 ± 0.18	0.92 ± 0.22	25.03 ± 0.55	0.62 ± 0.51	0.5 ± 0.14	35.87	21.02 ± 0.17	0.93 ± 0.2	24.44 ± 0.51	0.75 ± 0.57	0.54 ± 0.13	38.77	0.5	LSB, Y2
COMA-10.7441	195.551728	27.151625	21.69 ± 0.15	0.74 ± 0.21	24.62 ± 0.62	0.39 ± 0.47	0.52 ± 0.13	5.03	21.12 ± 0.15	0.68 ± 0.18	23.86 ± 0.59	0.36 ± 0.55	0.46 ± 0.12	178.49	0.87	LSB, > RS
COMA-10.7508	195.283688	27.076344	21.72 ± 0.15	0.73 ± 0.21	24.6 ± 0.63	0.1 ± 0.46	0.74 ± 0.13	48.81	21.43 ± 0.16	0.71 ± 0.19	24.24 ± 0.62	0.06 ± 0.56	0.85 ± 0.13	58.59	0.57	LSB
COMA-10.7564	195.32216	26.761515	21.74 ± 0.2	1.01 ± 0.23	25.34 ± 0.54	1.02 ± 0.55	0.57 ± 0.14	159.69	21.73 ± 0.19	0.82 ± 0.23	24.86 ± 0.63	1.11 ± 0.59	0.67 ± 0.13	140.72	0.52	LSB
COMA-10.7634	195.30801	26.792051	21.77 ± 0.15	0.69 ± 0.2	24.54 ± 0.66	1.37 ± 0.46	0.73 ± 0.13	171.36	21.39 ± 0.16	0.65 ± 0.19	24.03 ± 0.64	1.06 ± 0.55	0.79 ± 0.12	161.72	0.68	LSB, > RS

Table 2: Catalogue of Coma cluster galaxies with structural parameters from GALFIT analysis. This is an example page from the complete catalogue which is available online. The columns are (1): Galaxy ID, written to indicate the corresponding field, (2) and (3): Galaxy position (RA and Dec, respectively) in degrees (J2000), (4)–(9): and (10)–(15): are the total AB magnitude, circularized effective radius, mean surface brightness within the effective radius, Sérsic index, axial ratio (all with corresponding uncertainties derived following the description in the text), and position angle from  $V$  and  $R$ -band analysis, respectively. We have applied  $K$ -correction and Galactic extinction and Galactic extinction correction to our photometry.  $PA$  is measured East from North, (16): Galaxy colour obtained from SExtractor analysis, (17): comments about galaxy, starting with surface brightness category as defined in Section 6 (HSB, ISB or LSB), galaxies with colours redder than the  $1\sigma$  intrinsic scatter around the red-sequence are identified with >RS as explained in the text, identifier from the literature – Identifier from [Godwin et al. \(1983\)](#) and tidal features – (I: interacting; D: disturbed morphology; JF: Jelly-fish; R: Rings; P: Plumes; S: Shells)

ID	RA	Dec	$V$	$R_{eV}$	$\langle \mu_{\text{eff},V} \rangle$	$n_V$	$q_V$	$PA_V$	$V - R$
(1)	[Degree]	[Degree]	[mag]	[kpc]	[mag arcsec <sup>-2</sup> ]	(7)	(8)	[deg]	[mag]
(1)	(2)	(3)	(4)	(5)	(6)	(7)	(8)	(9)	(10)
COMA_14_1859	195.21524	28.871029	19.21 ± 0.16	2.41 ± 0.21	24.69 ± 0.25	0.51 ± 0.47	0.95 ± 0.13	74	0.52
COMA_23_2058	194.72876	28.65372	19.32 ± 0.16	2.3 ± 0.21	24.7 ± 0.25	0.32 ± 0.47	0.36 ± 0.13	156	0.47
COMA_30_2126	194.51813	27.056221	19.36 ± 0.15	2.1 ± 0.2	24.54 ± 0.26	1.11 ± 0.46	1.0 ± 0.13	83	0.46
COMA_33_2937	194.4494	28.542898	19.79 ± 0.17	2.03 ± 0.22	24.9 ± 0.29	1.24 ± 0.5	0.94 ± 0.14	15	0.44
COMA_14_3083	195.15186	28.930553	19.87 ± 0.17	1.91 ± 0.21	24.84 ± 0.29	1.05 ± 0.49	0.71 ± 0.13	179	0.47
COMA_32_3240	194.50377	27.88233	19.95 ± 0.18	2.08 ± 0.22	25.11 ± 0.3	0.95 ± 0.52	0.91 ± 0.14	56	0.39
COMA_12_3266	195.17593	28.164309	19.96 ± 0.17	1.84 ± 0.21	24.85 ± 0.3	1.21 ± 0.49	0.84 ± 0.13	21	0.45
COMA_42_3597	193.80339	27.786472	20.1 ± 0.16	1.62 ± 0.21	24.71 ± 0.32	1.01 ± 0.48	0.76 ± 0.13	92	0.46
COMA_41_3676	193.95773	27.398582	20.13 ± 0.19	2.04 ± 0.23	25.25 ± 0.31	1.13 ± 0.54	0.99 ± 0.14	80	0.36
COMA_24_3717	194.97047	28.7967	20.15 ± 0.15	1.5 ± 0.21	24.6 ± 0.34	1.02 ± 0.46	0.7 ± 0.13	88	0.5
COMA_31_3861	194.49976	27.619015	20.21 ± 0.17	1.74 ± 0.22	24.98 ± 0.32	1.08 ± 0.5	0.99 ± 0.14	120	0.46
COMA_32_3906	194.32854	28.154984	20.23 ± 0.16	1.53 ± 0.21	24.72 ± 0.34	1.0 ± 0.48	0.81 ± 0.13	63	0.38
COMA_30_3930	194.60199	26.745077	20.24 ± 0.16	1.58 ± 0.21	24.81 ± 0.34	0.86 ± 0.49	0.9 ± 0.13	12	0.55
COMA_22_4042	194.72652	28.08718	20.29 ± 0.17	1.64 ± 0.22	24.93 ± 0.34	0.84 ± 0.5	0.92 ± 0.14	157	0.48
COMA_12_4296	195.2982	28.145302	20.41 ± 0.22	2.11 ± 0.24	25.6 ± 0.33	1.04 ± 0.58	0.71 ± 0.15	47	0.46
COMA_22_4410	195.06532	28.029459	20.45 ± 0.17	1.5 ± 0.22	24.9 ± 0.36	1.08 ± 0.5	0.69 ± 0.14	37	0.54
COMA_34_4521	194.25638	28.87275	20.5 ± 0.18	1.58 ± 0.22	25.06 ± 0.35	0.85 ± 0.51	0.75 ± 0.14	36	1.18
COMA_32_4544	194.46745	28.105352	20.51 ± 0.18	1.58 ± 0.22	25.07 ± 0.35	0.83 ± 0.52	0.92 ± 0.14	70	0.33
COMA_41_4570	193.86931	27.684788	20.52 ± 0.18	1.55 ± 0.22	25.05 ± 0.36	0.75 ± 0.51	0.62 ± 0.14	158	0.41
COMA_22_4600	194.71304	28.13771	20.54 ± 0.18	1.58 ± 0.22	25.1 ± 0.36	0.63 ± 0.52	0.84 ± 0.14	72	0.52
COMA_30_4629	194.23543	27.045115	20.55 ± 0.17	1.48 ± 0.22	24.96 ± 0.36	0.76 ± 0.5	0.99 ± 0.14	60	0.64
COMA_22_4735	194.77484	27.97042	20.6 ± 0.18	1.56 ± 0.22	25.13 ± 0.36	0.29 ± 0.52	0.46 ± 0.14	21	0.55
COMA_22_5227	194.9666	27.82323	20.79 ± 0.21	1.71 ± 0.24	25.52 ± 0.37	0.44 ± 0.57	0.33 ± 0.14	42	0.71
COMA_31_5314	194.59314	27.38581	20.82 ± 0.2	1.53 ± 0.23	25.31 ± 0.38	0.78 ± 0.54	0.76 ± 0.14	100	0.45
COMA_12_5647	195.48859	28.138306	20.95 ± 0.22	1.73 ± 0.25	25.71 ± 0.38	1.03 ± 0.6	0.95 ± 0.15	161	0.53
COMA_23_5706	194.8023	28.353645	20.97 ± 0.23	1.8 ± 0.25	25.82 ± 0.38	1.06 ± 0.61	0.99 ± 0.15	39	0.29
COMA_13_6651	195.3371	28.539967	21.34 ± 0.25	1.7 ± 0.26	26.05 ± 0.42	0.7 ± 0.64	0.77 ± 0.16	46	0.4
COMA_32_6911	194.60907	27.867151	21.45 ± 0.25	1.55 ± 0.26	25.96 ± 0.44	1.01 ± 0.63	0.98 ± 0.15	122	0.28
COMA_22_6931	194.78117	28.13321	21.46 ± 0.27	1.73 ± 0.27	26.21 ± 0.43	1.02 ± 0.67	0.81 ± 0.16	133	0.5

**Table 3.** Newly discovered ultra-diffuse galaxies in the Coma cluster catalogued here for convenience. Columns are the same as in Table 2 although we only show parameters from the  $V$ -band.

- Kron R. G., 1980, *ApJS*, **43**, 305
- Kubo J. M., Stebbins A., Annis J., Dell’Antonio I. P., Lin H., Khiabani H., Frieman J. A., 2007, *ApJ*, **671**, 1466
- Lim S., Peng E. W., Côté P., Sales L. V., den Brok M., Blakeslee J. P., Guhathakurta P., 2018, *ApJ*, **862**, 82
- Mahajan S., Haines C. P., Raychaudhury S., 2011, *MNRAS*, **412**, 1098
- Mancera Pia P. E., Aguerri J. A. L., Peletier R. F., Venhola A., Trager S., Choque Challapa N., 2019, *Monthly Notices of the Royal Astronomical Society*, **485**, 10361052
- Martin G., et al., 2019, *MNRAS*, **485**, 796
- McConnachie A. W., 2012, *AJ*, **144**, 4
- Miyazaki S., et al., 2002, *PASJ*, **54**, 833
- Mobasher B., et al., 2001, *ApJS*, **137**, 279
- Moore B., Katz N., Lake G., Dressler A., Oemler A., 1996, *Nature*, **379**, 613
- Okabe N., Futamase T., Kajisawa M., Kuroshima R., 2014, *ApJ*, **784**, 90
- Owers M. S., et al., 2019, *The Astrophysical Journal*, **873**, 52
- Peng C. Y., Ho L. C., Impey C. D., Rix H.-W., 2010, *AJ*, **139**, 2097
- Plionis M., 1994, *ApJS*, **95**, 401
- Renzini A., 2006, *ARA&A*, **44**, 141
- Román J., Trujillo I., 2017, *MNRAS*, **468**, 4039
- Ruiz-Lara T., et al., 2018a, *MNRAS*, **478**, 2034
- Ruiz-Lara T., et al., 2018b, *MNRAS*, **478**, 2034
- Sales L. V., Navarro J. F., Peñafiel L., Peng E. W., Lim S., Hernquist L., 2020, *MNRAS*, **494**, 1848
- Schlafly E. F., Finkbeiner D. P., 2011, *ApJ*, **737**, 103
- Secker J., Harris W. E., Plummer J. D., 1997, *Publications of the Astronomical Society of the Pacific*, **109**, 1377
- Sérsic J. L., 1968, Atlas de galaxias australes
- Smith R. J., Lucey J. R., Hudson M. J., Allanson S. P., Bridges T. J., Hornschemeier A. E., Marzke R. O., Miller N. A., 2009, *MNRAS*, **392**, 1265
- Smith R. J., Lucey J. R., Price J., Hudson M. J., Phillipps S., 2011, *Monthly Notices of the Royal Astronomical Society*, **419**, 31673180
- Taylor M. B., 2005, in Shopbell P., Britton M., Ebert R., eds, *Astronomical Society of the Pacific Conference Series Vol. 347, Astronomical Data Analysis Software and Systems XIV*, p. 29
- Terlevich A., Caldwell N., Bower R., 2001, *Monthly Notices of the Royal Astronomical Society*, **326**, 1547
- Trujillo I., Graham A. W., Caon N., 2001, *MNRAS*, **326**, 869
- Wittmann C., et al., 2017, *MNRAS*, **470**, 1512
- Yagi M., Koda J., Komiyama Y., Yamanoi H., 2016, *ApJS*, **225**, 11
- Zabludoff A. I., Mulchaey J. S., 1998, *ApJ*, **496**, 39
- Zaritsky D., et al., 2019, *ApJS*, **240**, 1
- de Vaucouleurs G., 1948, *Annales d’Astrophysique*, **11**, 247
- de Vaucouleurs G., 1959, *Handbuch der Physik*, **53**, 275
- van Dokkum P. G., et al., 2015, *ApJ*, **804**, L26
- van der Wel A., et al., 2013, *ApJ*, **777**, L17

## APPENDIX A: COMPARISON WITH THE LITERATURE

In this appendix we compare results from our GALFIT analysis with results from the literature, starting with total magnitudes. The Coma cluster has been well-studied in both  $V$  and  $R$  bands to various photometric depths and azimuthal coverage (e.g. Terlevich et al. 2001; Mobasher et al. 2001; Adami et al. 2006; Eisenhardt et al. 2007; Yagi et al. 2016, etc.), mostly with SExtractor

analysis and in the Vega magnitude system. We apply an average correction of  $\sim 0.3$  to account for the systematic offset between magnitude estimates from SExtractor analysis and GALFIT 2D-decomposition (e.g. Häussler et al. 2007; van der Wel et al. 2013, etc) and apply the appropriate corrections between the Vega and AB magnitude systems:  $R_{AB} = R_{VEGA} + 0.21$  and  $V_{AB} = V_{VEGA} + 0.02$  (Blanton & Roweis 2007). We also include recent results from the F606W *HST* study by Lim et al. (2018) where a handful of Coma cluster galaxies were analysed with GALFIT. Figure A1 shows how our total magnitude measurements compare with several studies from the literature (all in AB magnitude system) over  $\sim 12$  magnitudes in both  $V$  and  $R$  bands.

We also compare our measured effective radius  $R_e$  (Figure A2), Sérsic index  $n$  (Figure A3), axial ratio  $q$  (Figure A4), and position angle  $PA$  (Figure A5) with results from various literature sources including Gutiérrez et al. (2004); Hoyos et al. (2011); Yagi et al. (2016); Lim et al. (2018); Zaritsky et al. (2019). Generally, our measured galaxy structural parameters show good agreement with previous works from the literature bearing in mind the various set of assumptions<sup>5</sup> and the different nature of the data we have compared with<sup>6</sup>

This paper has been typeset from a  $\text{\TeX}/\text{\LaTeX}$  file prepared by the author.

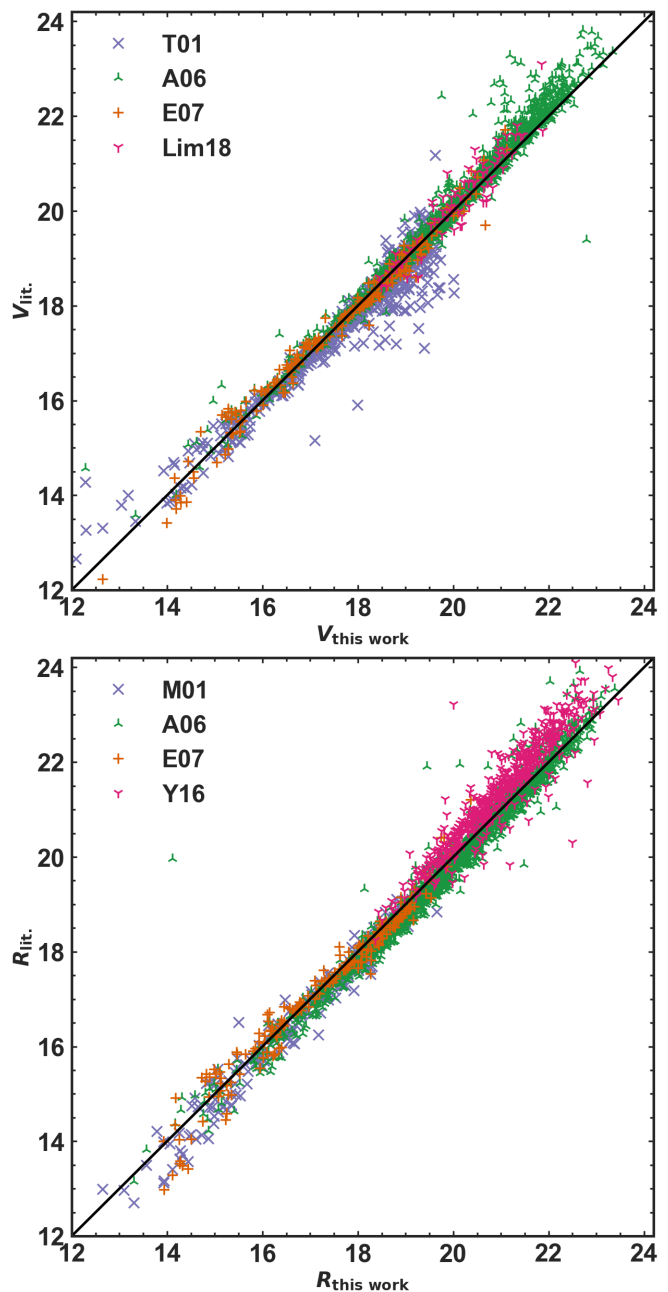


**Figure A1.** Comparison of total magnitudes from our GALFIT analysis in  $V$  and  $R$ -bands (*left and right panels*, respectively) with measurements from Mobasher et al. (2001, M01), Terlevich et al. (2001, T01), Adami et al. (2006, A06), Eisenhardt et al. (2007, E07), Yagi et al. (2016, Y16), and Lim et al. (2018, Lim18). There is a very good agreement between our measurements and the literature over  $\sim 12$  magnitudes. Note that we report systematically brighter magnitudes for faint, low surface brightness galaxies due to the magnitude correction we applied as discussed in the text.

<sup>5</sup> For example, some authors fixed  $n = 1$  in their GALFIT analysis and have adopted various methods in dealing with the background sky, both factors which affect the values of the modelled parameters significantly.

<sup>6</sup> Our comparison dataset include ground-based and *HST* data in several photometric bands with varying resolutions.



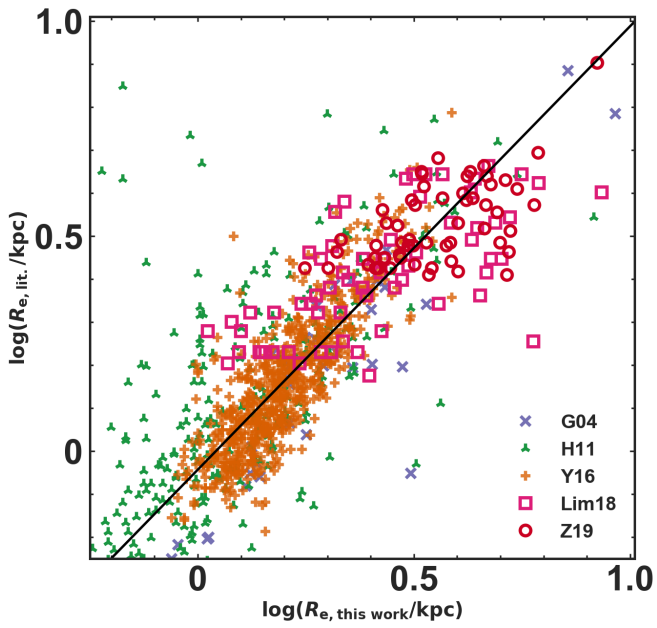


**Figure A2.** Comparison of galaxy sizes,  $R_e$ , with previous results from the literature as shown in the plot legend Gutiérrez et al. (2004, G04), Hoyos et al. (2011, H11), Yagi et al. (2016, Y16), Lim et al. (2018, Lim18), and Zaritsky et al. (2019, Z19).

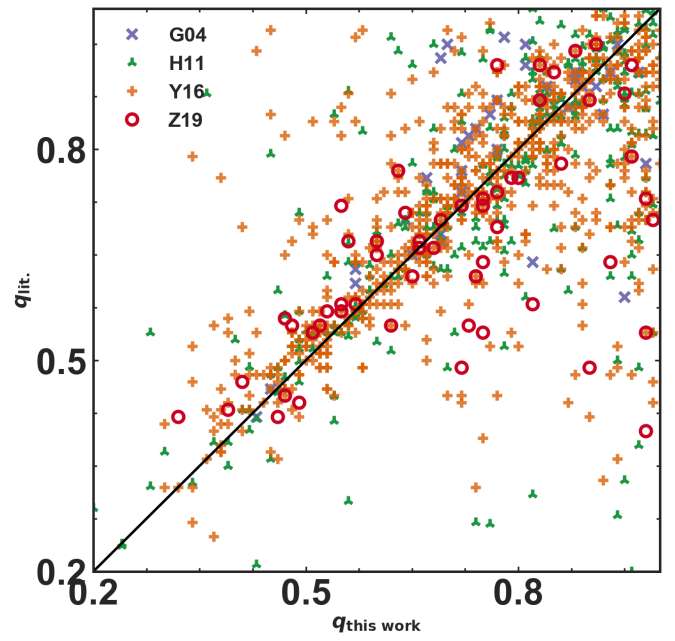


**Figure A4.** Same as in Figure A2 but showing galaxy axial ratios,  $q$ .

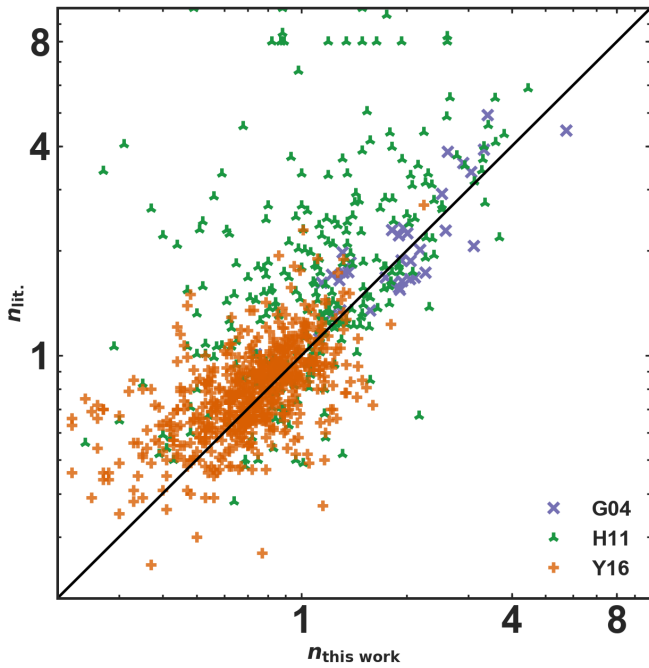


**Figure A3.** Same as in Figure A2 but showing galaxy Sérsic index,  $n$ .

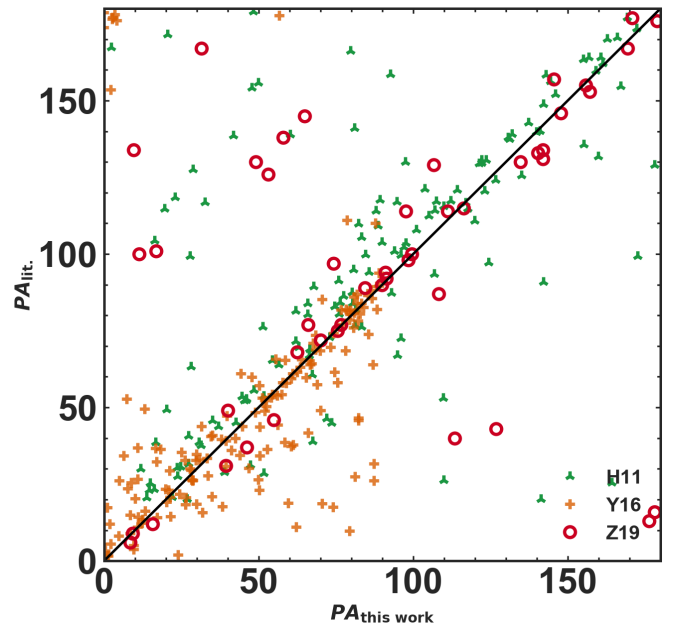


**Figure A5.** Same as in Figure A2 but showing galaxy position angles,  $PA$ .